

# Design of a Low-Cost Sustainable Energy Storage System Through Utilization of Compressed Air



**Major Qualifying Project Report  
submitted to the Faculty of the  
WORCESTER POLYTECHNIC INSTITUTE  
in partial fulfillment of the requirements for the  
Degree of Bachelor of Science by:**

Andrew Gray | ME | '20  
Robert James | ME | '20  
Hannah Mikkila | ME | '20  
Gavin Sabol | ME | '20

Advisor: Professor Robert Daniello

Sponsor: Claude-Reynald Lecorps | Atlas Prime NRG

## Abstract

In a world becoming progressively more dependent on electricity, it is increasingly difficult to build low-cost green energy systems that can match this need. Atlas Prime NRG has set out to solve this problem with the Compressed Air Renewable Integrated Energy System (CARIES) which strives to produce reliable low-cost green energy for remote parts of the world by using compressed air for long-term energy storage. The goal of this project was to design, model, and spec an air compressor that would be used in CARIES to intake air at atmospheric conditions and compress it to 3,000 psig. ANSYS simulations were used to guarantee structural integrity. The final design plans, CAD models, and specifications were delivered to Atlas Prime NRG.

The teams' compression device is a four-cylinder reciprocating compressor with a design RPM of 880. The number of cylinders allows for a reduced compression ratio which means that the pistons can perform work on the air without subjecting the cylinder to undue thermal and physical stress. Increasing the pressure also brings along an associated temperature rise in the air; in order to deal with the temperature increase, a heat exchanger is placed after each compression stage to cool the air to an acceptable temperature before the next stage. After the last compression cycle, the air is then run through a final heat exchanger and stored in pressure-rated scuba tanks.

# Table of Contents

<b>Abstract</b>	<b>1</b>
<b>Table of Contents</b>	<b>2</b>
<b>Table of Figures</b>	<b>5</b>
<b>List of Tables</b>	<b>9</b>
<b>Chapter 1 - Introduction</b>	<b>10</b>
<b>Chapter 2 - Background</b>	<b>11</b>
2.1 Energy in Haiti	11
2.2 Atlas Power CARIES System	11
2.3 Types of Air Compressors	12
2.3.1 Reciprocating Compressor	12
Oil-free Reciprocating Compressors	14
Teflon O-Ring	15
Advantages of Reciprocating Compressors	15
Disadvantages of Reciprocating Compressors	16
2.3.2 Screw Compressor	16
Oil-free Screw Compressors	18
Advantages of Screw Compressors	18
Disadvantages of Screw Compressors	19
2.3.3 Centrifugal Compressor	19
Advantages of Centrifugal Compressors	21
Disadvantages of Centrifugal Compressors	22
2.4 Commercially Available Compressors	22
<b>Chapter 3 - Design Process</b>	<b>24</b>
3.1 Specifications and Requirements	24

	3
3.2 Compressor Selection	24
3.2.1 Design Choice	25
3.3 Material selections	26
3.3.1 Cylinder Material selection	27
3.3.2 Crankshaft, Connecting Rod, and Master Rod Material Selection	29
3.3.3 Piston Material Selection	31
3.4 Component Selection	31
3.4.1 Valve Selection	31
3.4.2 Motor Selection	33
3.4.3 Bearing and Bushing Selection	34
3.4.4 Piston Ring Selection	35
3.4.5 Oil Lubrication Selection	36
3.5 Commercial Alternative Analysis	37
3.5.1 “YONG HENG” Paintball Compressor	38
3.5.2 Scuba Compressors	38
3.5.3 Reciprocating Compressor Disassembly	38
Connecting Rods, Piston Heads, and Piston Rings	39
Crankshaft	42
<b>Chapter 4 - Methodology and Calculations</b>	<b>43</b>
4.1 Assumptions	43
4.2 Initial Sizing from Volumetric Efficiency	43
4.2.1 Calculating Cylinder Stresses from a Thick-Walled Model	44
4.2.2 Cooling	45
4.2.3 Motor Specifications from Torque	47
4.2.4 Overall Efficiency	48
<b>Chapter 5 - CAD</b>	<b>49</b>

	4
<b>Chapter 6 - Failure Analysis (ANSYS)</b>	<b>53</b>
<b>Chapter 7 - Results</b>	<b>55</b>
7.1 Cost Analysis	55
7.2 Recommendations	56
7.2.1 Design Changes	57
7.2.2 Bushing and Ball Bearings	57
7.3 Commercial Alternatives	57
<b>References</b>	<b>60</b>
<b>Appendix A: Glossary</b>	<b>64</b>
<b>Appendix B: Cylinder Material Properties</b>	<b>65</b>
<b>Appendix C: Crankshaft Material Properties</b>	<b>73</b>
<b>Appendix D: CAD</b>	<b>76</b>
<b>Appendix E: Failure Analysis of Cylinders</b>	<b>78</b>
<b>Appendix F: Failure Analysis of Piston</b>	<b>83</b>
<b>Appendix G: Failure Analysis of Connecting Rods</b>	<b>90</b>

## Table of Figures

Figure	Title
1	CARIES Diagram
2	Reciprocating Compressor Diagram
3	Piston Ring Diagram
4	Reciprocating Compressor O-ring
5	Screw Compressor Diagram
6	Screw Geometry Diagram
7	Centrifugal Compressor Diagram
8	Multi - Stage Centrifugal Compressor Diagram
9	Compressor Type: Flow Rate vs. Pressure Ratio
10	Trunk-piston Compressor
11	Suction Valve
12	Air Compressor Filter
13	Poppet Valve
14	Drawings of Forward Ball Valve (left) and Reverse Ball Valve (right)
15	AC Motor- 7 ½ HP
16	Bushings and Bearing
17	Ball Bearing-35mm Diameter
18	Brass Bushing-½" Diameter
19	Compressor Piston with Grooves for Piston Rings
20	Lubrication Diagram
21	Connecting Rods, Piston Heads, and Piston Rings
22	Piston Bottom View

23	Piston Side View
24	Piston Ring Assembly
25	Crankshaft Assembly
26	Volumetric Sizing Equations
27	Clearance Visualization
28	Radial Stress in the Cylinders as a Function of Radii and Pressures
29	Hoop Stress in the Cylinders as a Function of Radii and Pressures
30	Cross Section of Heat Exchangers at Stage 1 Exit (left) and Stage 4 Exit (right)
31	Nusselt Number Correlation for First Cooling Device
32	Torque on Motor vs Crank Angle
33	Theoretical Power Per Stage
34	Air Compressor Rendering
35	All Stage Cross Sectional View
36	Compressor Casing
37	Major Offset Rotational Pin
38	Heat Exchanger cross Sectional View
39	Heat Exchanger System
40	Nuvair Coltri MCH13 Compact Evo Compressor
41	Toolots Scuba High Pressure Air Compressor
42	Nuvair COLTRI MCH6 Portable High Pressure Compressor
43	Carbon Steel, AISI 1095 Fatigue Strength Graph
44	Low Alloy Steel, AISI 5140 Fatigue Strength Graph
45	Low Alloy Steel, AISI 4140 Fatigue Strength Graph
46	Cast Iron, Pearlitic Malleable Fatigue Strength Graph

47	Low Alloy Steel, 300M Fatigue Strength Graph
48	Low Alloy Steel, AISI 9260 Fatigue Strength Graph
49	Carbon Steel, AISI 1095 Fatigue Strength Graph
50	Piston Design Stages 1 through 4
51	Cylinder Chamber Stages 1 through 4
52	Side View of Cylinder Chamber Highlighting Fins
53	Cylinder Chamber Top View Highlighting Valve Holes
54	Connecting Rod Design Stages 2-4
55	Crankshaft Design
56	Stage 1 Cylinder ANSYS Deformation
57	Stage 2 Cylinder ANSYS Deformation
58	Stage 3 Cylinder ANSYS Deformation
59	Stage 4 Cylinder ANSYS Deformation
60	Stage 1 Cylinder ANSYS Stress
61	Stage 2 Cylinder ANSYS Stress
62	Stage 3 Cylinder ANSYS Stress
63	Stage 4 Cylinder ANSYS Stress
64	Piston Stage 1 Deformation
65	Piston Stage 2 Deformation
66	Piston Stage 3 Deformation
67	Piston Stage 4 Deformation
68	Piston Stage 1 Stress
69	Piston Stage 2 Stress
70	Piston Stage 3 Stress

71	Piston Stage 4 Stress
72	Master Rod to Piston Deformation Stage 1
73	Connecting Rod to Piston Deformation Stage 2
74	Connecting Rod to Piston Deformation Stage 3
75	Connecting Rod to Piston Deformation Stage 4
76	Master Rod to Piston Stress Stage 1
77	Connecting Rod to Piston Stress Stage 2
78	Connecting Rod to Piston Stress Stage 3
79	Connecting Rod to Piston Stress Stage 4
80	Master Rod Deformation Stage 1
81	Connecting Rod Deformation Stage 2
82	Connecting Rod Deformation Stage 3
83	Connecting Rod Deformation Stage 4
84	Master Rod Stress
85	Connecting Rod Stress Stage 2
86	Connecting Rod Stress Stage 3
87	Connecting Rod Stress Stage 4

## List of Tables

<b>Table</b>	<b>Title</b>
1	Cylinder Material Properties
2	Cylinder Material Weight Matrix
3	Cylinder Weighted Ranked Material Matrix
4	Crankshaft Material Properties
5	Material Weight Matrix for Crankshaft
6	Crankshaft Weighted Rated Material Matrix
7	Heat Exchanger Parameters
8	Cylinder Load from Maximum Pressure in Chamber Ansys Simulation Results
9	Piston Load from Maximum Pressure in Chamber Ansys Simulation Results
10	Connecting Rod Load From Piston Head Ansys Simulation Results
11	Connecting Rod Perpendicular Load Ansys Simulation Results
12	Parts Quantity and Cost List
13	Carbon Steel, AISI 1095 Material Properties
14	Low Alloy Steel, AISI 5140 Material Properties
15	Low Alloy Steel, AISI 4140 Material Properties
16	Cast Iron, EN GJMB 650-2 Material Properties
17	Low Alloy Steel, 300M Material Properties
18	Low Alloy Steel, AISI 9260 Material Properties
19	Carbon Steel, AISI 1095 Material Properties

## **Chapter 1 - Introduction**

Developing and maintaining low-cost energy systems in remote areas has been a challenge for green energy system manufacturers for several years. In addition to creating a system which can run for years with minimal human interference, there is also a challenge in designing this system at a reasonable cost. Atlas Prime NRG believes it has the solution to this problem with the Compressed Air Renewable Integrated Energy Storage (CARIES), which strives to produce low-cost green energy in low-income and remote parts of the world (Atlas Prime NRG, 2019). CARIES provides low-cost green energy by utilizing solar insolation to produce heat and electricity; the excess heat then provides the energy to compress and store air at 3,000 psig. This project will use compressed air as long term energy storage similar to a battery by compressing air from atmospheric pressure to 3000 psig at a minimum rate of 105 standard cubic feet per hour.

## Chapter 2 - Background

Today in industry, reciprocating, screw, and centrifugal air compressors are all commonly used. In order to design the best compressor for CARIES, it was important to evaluate the positives and negatives of these compressor designs. In addition, it was important for the team to conduct an analysis of commercially available compressors that met Atlas Prime NRG's requirements. This analysis helped the team design a compressor that aligned with existing industry standard best practices.

The CARIES system uses compressed air as long-term energy storage. Many places in the world, such as Haiti, struggle to reliably produce power. The integration of an air compressor in the CARIES energy system will ideally provide more places in the world with easier access to energy.

### 2.1 Energy in Haiti

Due to its high levels of poverty and political instability, Haiti has been faced with an energy problem for many years (export.gov, 2019). Roughly 80% of Haiti's energy is produced from imported fossil fuels, however, these resources are poorly managed and result in routine blackouts across the country (export.gov, 2019). Only 25% of Haiti's population has access to electricity, although even for them it is rare to have power for an entire day (Beckett, 2019). Wealthy families and businesses tend to spend large amounts of money on personal generators while poor families are left with using natural resources like wood and charcoal (Beckett, 2019).

The electricity problem in Haiti has been at the forefront of Haitian politics for many years. Recently, president Jovenel Moise pledged to bring twenty-four hours of electrical service to Haiti (Beckett, 2019). This is an important goal for Haiti because they will continue to struggle to develop if they do not find a way to incorporate a reliable source of electricity. In addition to the lack of development, it puts the country at risk. Haiti is in a position where it is susceptible to natural disasters like hurricanes and earthquakes. During these natural disasters, it's crucial to have an energy system robust enough to avoid damage during the disaster and aid in the recovery of the country and its people in the aftermath.

### 2.2 Atlas Power CARIES System

The acronym CARIES is short for Compressed Air Renewable Integrated Energy Storage. CARIES is simply a system that stores energy in the form of compressed air. Since the system is solar powered, it can only produce energy during hours of sunlight. In order

for the system to be operational outside of the hours of sunlight, CARIES compresses and stores air during the day while the solar collectors are generating electricity. Then, when it's dark out, the system will use the compressed air to continue generating energy. The purpose of CARIES is to provide long term storage that allows for twenty-four hour a day operation (Atlas Prime NRG, 2019).

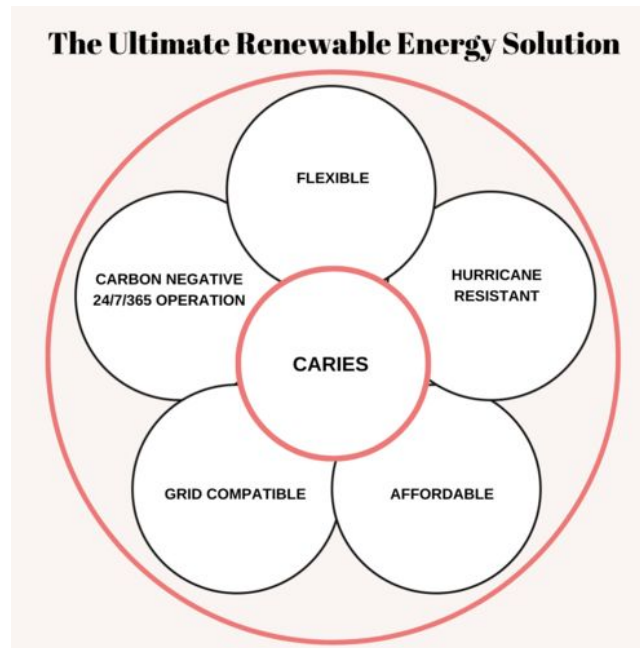


Figure 1, CARIES Diagram (Atlas Prime NRG, 2019)

## 2.3 Types of Air Compressors

The first step in designing an air compressor for CARIES is selecting the best type of compressor. Three types of air compressors have been identified for potential use: a reciprocating compressor, a screw compressor, and a centrifugal compressor.

### 2.3.1 Reciprocating Compressor

Reciprocating compressors are positive-displacement compressors and often considered the most commonly used type of air compressor (Parr, 2011). Reciprocating compressors work by pushing air up and down using a crankshaft that is typically powered by an external motor as seen in *Figure 2* below (Arfalk, 2014). The piston pushes air into a smaller volume to increase pressure, which also causes the temperature of the air to increase (Scott, 2017). Some reciprocating compressors consist of multiple stages that cool the air between each stage before compressing the air again using a smaller piston. This allows the compressor to be made using low-cost materials because the air is getting cooled in between each compression cycle. This also permits higher pressures to be

reached incrementally while decreasing the total heat produced during each stage. (Parr, 2011).

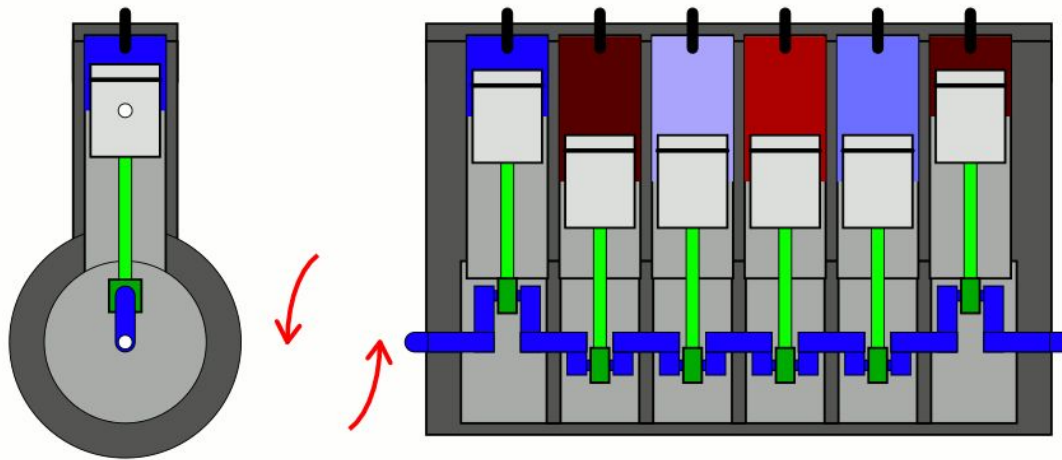


*Figure 2, Reciprocating Compressor Diagram (Frey, 2015)*

As the piston moves down gas fills the cylinder from a timed inlet valve. The valve then closes and the piston moves up, compressing the air and resulting in higher pressure. As the piston reaches the top of its stroke, a timed outlet valve opens and allows the compressed air to escape. This gas will either be moved to a compressed air storage tank or cooled through the application of an intercooling system. Finally, this air is run through additional stages in order to achieve the desired pressure while limiting the excess heat produced from the operation. The gas must be stored or used immediately after its final compression stage in order to prevent depressurization and ensure that the reciprocating compressor is running efficiently (Scott, 2017).

The piston head itself is the driving force of the entire compressor, and thus is carefully constructed to ensure that the volumetric losses occurring in the compression chamber itself are minimal. According to the University of Windsor, in order to ensure adequate sealing, cast iron piston rings are placed in machined ring grooves on top of the piston head (2019). *Figure 3* below depicts the piston rings conventionally used - the compression ring, wiper ring and oil ring.

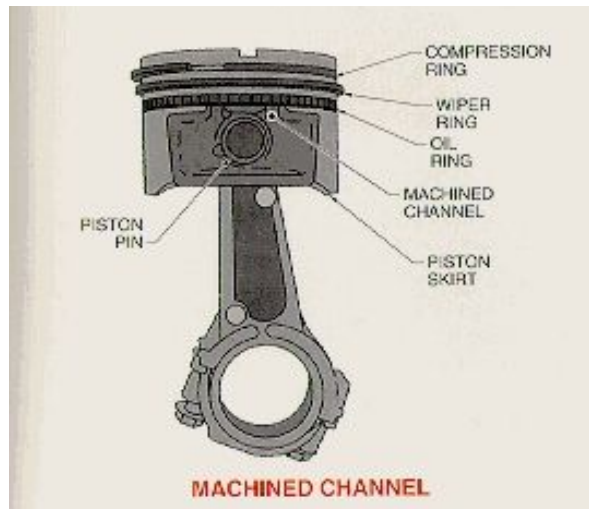


*Figure 3, Piston Ring Diagram (University of Windsor, 2019)*

The ring located at the top is the compression ring and is responsible for sealing the chamber to ensure that a limited amount of air leakage is present during compression. This ring uses the immense pressure built up in the chamber to create a seal by allowing pressurized air to enter the ring groove and force the ring up against the wall of the cylinder. This compression ring is also the closest ring to the compressed air, and thus achieves the highest operating temperature. As a result of the compression ring's contact with the piston wall, seventy percent of the heat created in the compression chamber is transferred to the cylinder's walls, allowing for the compression chamber to be cooled.

The second ring located from the top of the piston head is the wiper ring. It utilizes a tapered face to clean the cylinder wall of excess oil, as well as act as a backup sealant ring for any air that gets past the compression ring. Additionally, the tapered face design creates a passage between the wiper ring and oil ring allowing excess oil collected by the wiper ring to be removed. The oil ring is located below the wiper ring and typically is manufactured with holes or slots cut into the center of the ring. This allows for the oil that collects around the oil ring to be transported back to the oil reservoir and eventually reused. The oil ring is pressed against the piston wall due to the high pressure of the compressed air, and assists the wiper ring to eliminate the excess oil on the chamber walls to ensure a consistent oil layer.

### **Oil-free Reciprocating Compressors**

According to Quincy Compressors, an oil-free reciprocating compressor or non-lubricated reciprocating compressor can guarantee zero air contamination from oil lubricants while the system is operating (2019). Oil is typically used to help reduce the wear of parts, however, oil-free compressors replace oil with a Teflon or carbon ring. The

major problem that occurs with oil-free compressors is this absence of oil results in more heat generation. In some cases the dry arrangement reaches twice the temperature of its lubricated counterpart. As a result of these high temperatures, oil-free compressors have a greater number of compression stages and cooling systems to keep the operating temperature of the system as low as possible. Cooling is typically done by circulating coolant through a system of tubes to draw heat away from the mechanical parts.

Although proper cooling allows for an oil-free reciprocating compressor to operate efficiently, the overall lifespan of the product is decreased due to the increased wear. Teflon coatings wear away at a faster rate than oil and also require vigilant maintenance in order to minimize internal damage. As a result, teflon rings typically have higher maintenance costs over time (Quincy Compressor, 2019).

### **Teflon O-Ring**

Teflon O-rings are used in place of oil in non-lubricated reciprocating compressors. As the piston slides back and forth inside the cylinder, the Teflon O-ring helps to seal the surface of the cylinder (Parker, 2018). This can be seen in the figure below.

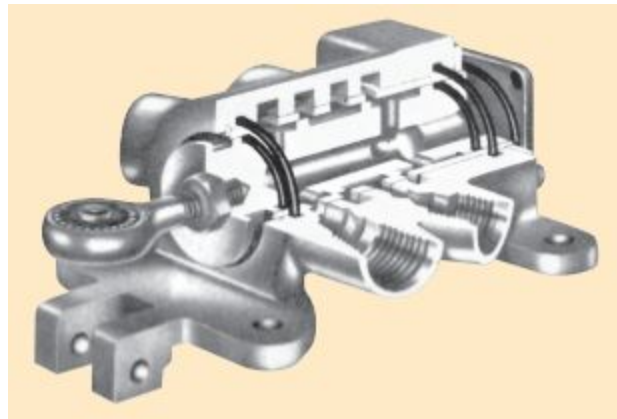


*Figure 4, Reciprocating Compressor O-ring (Parker, 2018)*

Most oil-free compressors use Teflon or PTFE (polytetrafluoroethylene) O-rings because of their ability to work well at high temperatures. Additionally, their low coefficient of friction makes them an ideal material (Reading Plastic, 2019). Finally, Teflon O-rings are easy to install, are less likely to twist during installation, and are less likely to stick after long storage (Parker, 2018).

### **Advantages of Reciprocating Compressors**

Reciprocating compressors are the best fit for systems that need high compression and have low flow rates (Wildenrad, 2019). These compressors also offer the advantage of

being comparatively inexpensive and more efficient especially when designed with multiple stages (Schneider Electric, 2011). As a result of reciprocating compressors being the most commonly used compressor, they generally have low maintenance costs, are well designed, and easy to install. (Wildenrad, 2019). Due to their simplicity and high usage rates in industry, reciprocating compressors typically don't require a specialist to conduct repairs, helping to keep maintenance prices low (Schneider Electric, 2011). Finally, reciprocating compressors typically do not have oil carryover, which is when oil passes through filters and gets into discharge pipes causing problems (CompressorWise, 2019).

### **Disadvantages of Reciprocating Compressors**

While reciprocating compressors appear to have a lot of positive design aspects, they come with a few drawbacks. Reciprocating compressors can be very large and take up a lot of space. Additionally, reciprocating compressors can induce a high amount of vibration requiring them to be built on solid concrete foundations in order to avoid damage to both the compressor and its surrounding area (Schneider Electric, 2011).

Additional drawbacks include valve leakage, tail rod failure, and pulsation (Frank Lees, 2012). Leakage in the discharge valve is a common malfunction and is caused by an increase in temperature of the valve due to improper cooling. As a result, volumetric capacity of the cylinder chamber may fall and cause discharge pressures and temperatures to be abnormal. In this scenario, intake pressure rises while discharge pressure falls creating a very inefficient system. Failure of the tail-rod can be dangerous and potentially deadly. This mechanical failure occurs when the tail rod of the piston breaks off from the piston head resulting in the piston head launching out of the device at a very high speed. To prevent this mechanical failure, it is necessary to perform surface hardening and inspection of all components to guarantee safe operation. Finally, pulsation occurs when compressed air is discharged into the cooling system. This creates resonance that can severely damage mechanical equipment connected to the compressor.

### **2.3.2 Screw Compressor**

A screw compressor involves two rotating and interlocking screws and is made up of a "male" and "female" rotor as seen in *Figure 5* below. The male rotor consists of a number of lobes which interlock with the corresponding flutes, or valleys, on the female rotor. The number of lobes and flutes vary depending on the final pressure required by the system. The industry standard is to ensure a higher number of flutes than lobes in order to maximize the efficiency of the compressor's operation (GardnerDenver, 2019). The male and female rotors turn in opposite directions drawing in air through a suction valve located on the top portion of the compressor.

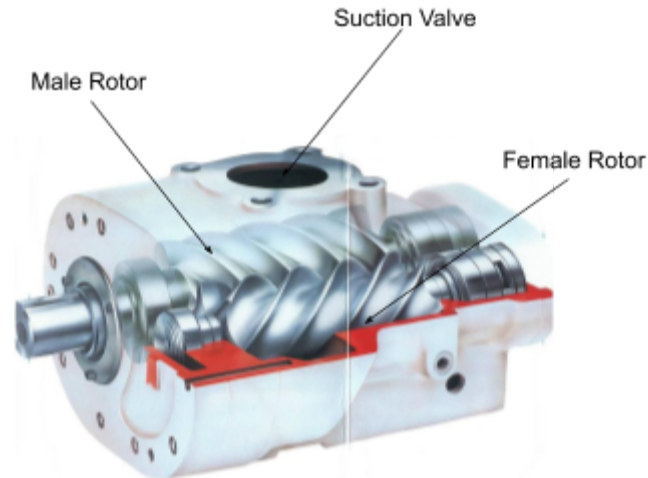


*Figure 5, Screw Compressor Diagram (Atula, 2015)*

The male lobes basically act as a piston. They roll down the female flutes, trapping air in the gaps created by the interlocking geometries. *Figure 6* below depicts a cross section of a typical male and female screw combination.

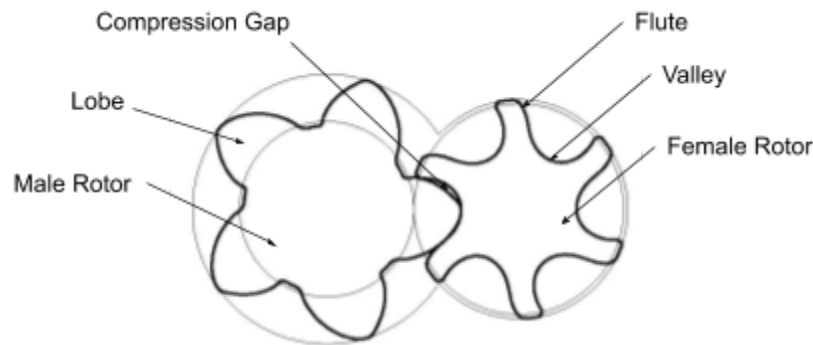


*Figure 6, Screw Geometry Diagram (Stosic and Hanjalic, 1997)*

As seen in the figure above, the larger protruding lobes fit into the valleys between the flutes while leaving a small pocket of free space. As air is suctioned into the compressor, it moves along the screws and fills this empty space. The rapid decrease in volume that the air experiences creates the subsequent pressure increase. As air moves along the lobes and valleys further down the screw, it becomes trapped between the geometries of the male and female screws, and increases overall pressure until it is discharged at a final outlet pressure (Atlas Copco, 2019).

Most lubricated screw compressors use cold oil to reduce operating temperature and to cool the rotors (The WC, 2019). Additionally, screw compressors have a very specific operation speed. If the compressor is running too fast it may reach hazardous

temperatures, but if it is running too slow there is a risk of air leakage which will decrease the compressor's efficiency. In order to optimize the screw compressor's performance, it's important to find a medium rotor speed (Atlas Copco, 2019).

### **Oil-free Screw Compressors**

Oil-free screw compressors do not use oil which is typically required to seal the compressor and to minimize leakage. Without oil, these screw compressors require highly precise tolerancing which results in higher costs and more complex machining operations. As the screw compressor operates, the air inside of the compressor increases in temperature and results in thermal expansion of the screws. The subsequent swelling of the metal caused by the temperature increase can eliminate the toleranced gaps and cause the metal rotors to come in contact with each other. Ultimately, this increase in friction and heat can cause mechanical failure of the compressor as the lobes could potentially weld together and cause the compressor to seize (The WC, 2019).

Oil-free screw compressors are cooled with water. This is less efficient than the oil alternative because water cannot directly contact the screws, and therefore cannot cool them as effectively. As a result, a material that can withstand higher temperatures and pressures may need to be used. Additionally, as a result of the thermal limitations of a water cooling system, an oil-free screw compressor will not be able to produce as high pressures as their lubricated counterparts.

### **Advantages of Screw Compressors**

Screw compressors have several advantages over other types of compressors. Screw compressors can be up to 25-30% more efficient than reciprocating compressors, however, the efficiency of a screw compressor is heavily dependent on how close the screws are during operation (Ebrahimi, 2019). This high efficiency is also due in part to the compressor's ability to process large amounts of air while running on a 100% continuous duty cycle (VMAC Air Innovated, 2019). Additionally, screw compressors have minimal vibration resulting in a much quieter compressor than other types of compressors (Schneider Electric, 2011). When comparing a screw compressor to a reciprocating compressor of similar output performance, the screw compressor will typically be much smaller in size. Additionally, screw compressors generally have better air quality than reciprocating compressors assuming the air filter is changed regularly (Ebrahimi, 2019).

In regards to their design, screw compressors lack a large number of moving parts which facilitates low maintenance and operational costs. This is due in part to how oil-injected screw compressors use the lubricant to seal the oil into the screws and allow for optimal running conditions (AshAir, 2019). Additionally, by having fewer moving parts

and less maintenance requirements, the compressor will typically have a longer lifetime as there is a major reduction in stresses imparted on the components. As a result, dangerous failures are very rare due to the simpler design and fewer points of failure (AshAir, 2019). The use of lubricating oil as a sealant also provides advantages because it eliminates the need for components like teflon rings (VMAC Air Innovated, 2019). This design simplifies routine maintenance since oil and filters are the only components that need replacement. Finally, the screws are very durable and are designed to last for up to 10 years (Dunning, 2017).

### **Disadvantages of Screw Compressors**

Although screw compressors are capable of similar performance to reciprocating compressors, there are some disadvantages to this type of machine. First, due to the complex geometries of screw rotors, they can be very difficult to design and expensive to manufacture. Additionally, getting rotors to seal can be difficult, and if not properly sealed, the compressor can leak or the rotors could swell too much and force the compressor to malfunction. Screw compressors are also typically more expensive than reciprocating compressors. It is also important to note that Atlas's system needs to produce 80 cubic feet of air in 45 minutes (less than 2 cubic feet per minute), and screw compressors that produce less than 70 cubic feet per minute usually require more maintenance than a reciprocating compressor (Ebrahimi, 2019).

### **2.3.3 Centrifugal Compressor**

A centrifugal or turbomachinery compressor involves the use of a radial design. Air is led into the radial blades through a guided inlet valve. A force generated by the rotation of the radial blades allows for intake air to gravitate towards the center of the rotating blades, allowing this air to subsequently move radially through the rotating impeller and compress (Arfalk, 2014). The driving force for the compression process includes the increased air velocity in the intake stream and the resulting kinetic energy created within the system (FS-Elliott, 2019). Next, this high-velocity air is passed through a diffuser in order to decelerate it. Through Bernoulli's rule - the idea that pressure is inversely proportional to velocity squared - the kinetic energy from the slowed air is converted into potential energy in the form of high pressure compressed air (Dugan, 2019). *Figure 7* below provides a diagram of the basic components in a centrifugal compressor.

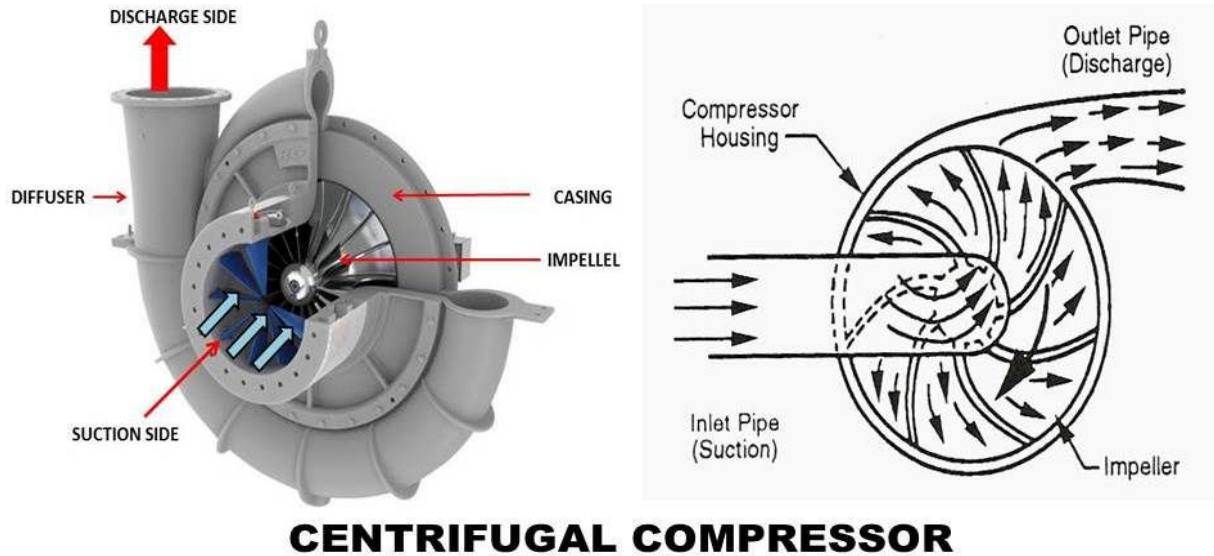


*Figure 7, Centrifugal Compressor Diagram (Mech4Study, 2017)*

As shown in the diagram, air is suctioned into the compressor through the guiding inlet valve highlighted in blue. The air is then fed into the spaces between the radial blades and spun at a high speed, typically averaging around 20,000 - 30,000 RPM, where it is then fed through the vaned diffuser and into the discharge pipe to create high pressure from the initial kinetic energy (Stewart, 2019).

To compress the air from atmospheric pressure to the desired final output pressure, multiple stages are commonly used especially in industrial applications such as supplying air in a manufacturing plant environment. A three-stage design, with intercoolers between each stage, is the most common type of centrifugal compressor because each stage is capable of a 2:1 or 3:1 compression ratio (Dugan, 2019). *Figure 8* below depicts a multi-stage centrifugal compressor.

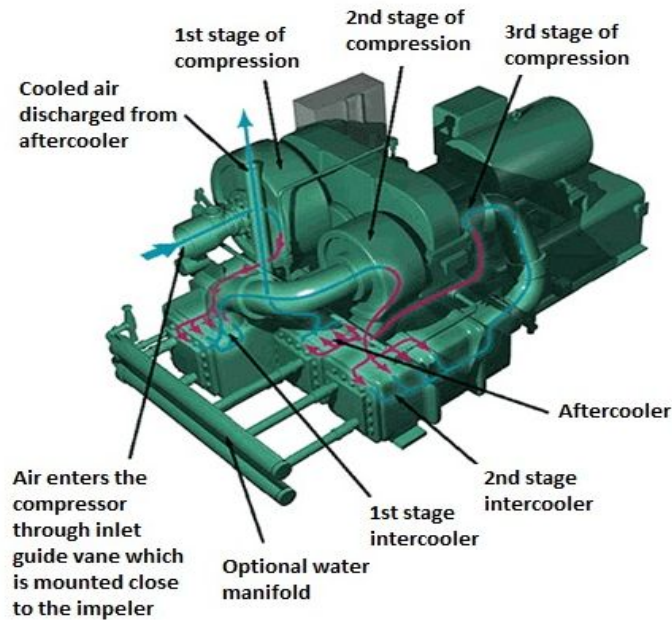


*Figure 8, Multi - Stage Centrifugal Compressor Diagram (Metrixvibration, 2019)*

Air enters through the guide vane and is then compressed and cooled throughout each stage. As seen above, each stage of compression requires differently sized radial blades with the largest blades typically in the first stage. This is a result of both the amount of air that needs to be compressed, and the large pressure differential in the atmospheric air and compressed air (Boyce, 2012).

### **Advantages of Centrifugal Compressors**

Centrifugal compressors have several advantages over other types of compressors, such as the design. The typical design specifications of a centrifugal compressor work well for applications that require a small change in pressure from the inlet to outlet, continuously compressed air supply, and large flow rates (Almasi, 2014). Centrifugal compressors are able to output flow rates that are far greater than that of a reciprocating compressor. Additionally, centrifugal compressors do not require a lot of material to manufacture, and thus can be light and more practical to design and manufacture for specialized applications (Samancioglu, 2016). Another advantage these types of compressors provide is that they have a small number of parts coming in close contact with each other. As a result, this lack of potential friction inside of the compressor makes them more reliable and require less maintenance in the long term (Mecholic, 2016). Another benefit of having low levels of internal friction is the ability of the compressor to be oil-free. Without oil, the output air will be of higher quality, and the design will not require air filtration systems which can help reduce costs (Ingersoll, 2019). Finally, as a result of

centrifugal compressors having very few moving parts, they will produce less noise and vibration compared to other alternatives (Schneider Electric, 2011).

### **Disadvantages of Centrifugal Compressors**

Centrifugal compressors have various disadvantages as well. The primary drawback of centrifugal compressors is their inflexibility in capacity and pressure ranges. Centrifugal compressors are commonly designed for large amounts of air and small pressure increases. When designing a compressor for an application that requires small flow rates or a large pressure increase - for example Atlas Prime's requirements to bring air from standard temperature and pressure and bring it to 3,000 psi - this machinery will struggle compared to alternative compressor types (Samancioglu, 2016). This is because a small radial blade will be less efficient at creating large pressure increases than a small piston head due to the lower power input required for the crankshaft to move the pistons. In addition, the radial blades inside the centrifugal compressor would be spinning at very high speeds and would require specialized bearings as well as sophisticated monitoring equipment in order to ensure clearances do not change from the initial design. In the event of a mechanical issue, specialized maintenance teams would be needed to resolve the problem (Schneider Electric, 2011).

Another drawback of centrifugal compressors is that they are more susceptible to the phenomena of surging, choking, and throttling. Surging can occur when the flow of air into the compressor is too low causing the pressure developed by the compressor to exceed the pressure at the discharge. This causes a reversal of airflow in the compressor, resulting in massive inefficiencies and a dramatic reduction in the compressor's output pressure (Mecholic, 2016). Surging is caused by throttling at the suction valve which causes the inlet flow to decrease. Conversely, throttling at the discharge valve will also cause surging which can cause the flow out of the compressor chamber to lower increasing the output pressure. Without immediate maintenance, the surging cycle will continue and cause mechanical damage to the compressor (MES, 2017). Choking can also damage the compressor. If the device is operating at a maximum flow rate and a low discharge pressure, the impeller and gas can begin to reach the same velocity causing the compressor to choke. This can cause severe damage in a multi-stage centrifugal compressor (Mecholic, 2016).

## **2.4 Commercially Available Compressors**

Currently, there are several different types of air compressors available for purchase. These compressors range from small and specific applications to others that are mass-produced and used for industrial applications. Since these companies have been

designing and manufacturing compressors for an extended period of time, it was important to understand the concepts and common practices already being used to make sure the designs the team came up with are modern, manufacturable, and efficient. Upon reviewing a variety of commercially available air compressors, the team proceeded to design an air compressor around the limitations and requirements given to them by Atlas Prime NRG.

## Chapter 3 - Design Process

The goal of this project was to design an air compressor to the specifications given by Atlas. In order to do this effectively, the team followed a series of steps to ensure the final design would meet the given requirements.

### 3.1 Specifications and Requirements

The first step for the team was to understand the requirements this air compressor needed to fulfill. Due to the design of the CARIES system, there were many limitations and requirements around which the team had to design. The purpose of this air compressor was to produce low-cost energy. Therefore, the compressor itself needed to be produced at a low cost to make this product accessible to the target market segment. According to Atlas Prime NRG, the air compressor portion of the system needed to be under \$2,000 in order to create an affordable product.

The air compressor will intake air at ambient conditions and compress it to 3,000 psig and 23°C. The air compressor needs to fill one 80 cubic foot scuba tank in under 45 minutes, requiring a flow rate of approximately 1.778 SCFM. The system is required to fill eight tanks every twenty-four hours. While this does not necessitate continuous operation, steady-state conditions are desirable in ensuring that there is enough surplus energy to meet this requirement, and will be equipped with 12 scuba tanks for sunny days where more energy is being produced. The air compressor is not required to be oil-free, however, Atlas Prime does not want oil or other substances to build up inside of the scuba tanks or the compressor itself in order to ensure the output air is of high quality. Finally, given the power generation capabilities of the CARIES system, the air compressor must be able to be powered with a maximum of 5 kW.

### 3.2 Compressor Selection

The second step for the team was to determine the best type of air compressor to meet the requirements provided by Atlas Prime. As stated above, the air compressor's major requirements were that it must have a flow rate of 1.778 SCFM, be able to compress air from atmospheric pressure to 3,000 psi, cost under \$2,000, and be able to operate 24 hours per day. In order to determine the best type of compressor for this application, the team analyzed their findings from *Chapter 2* and *Figure 9* below.

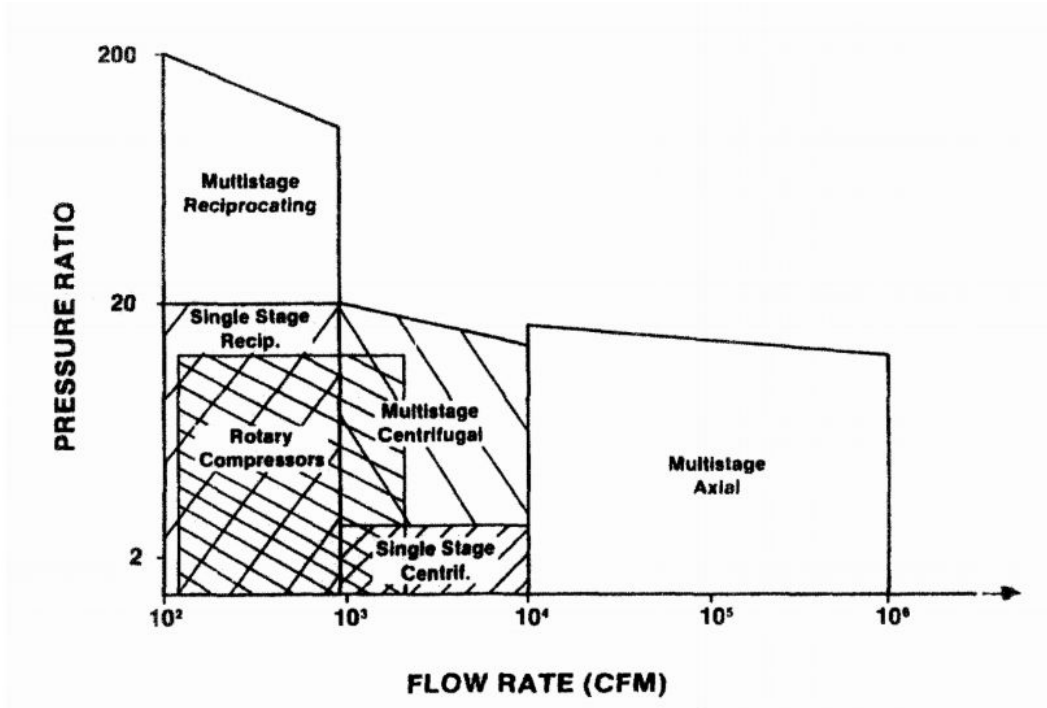


Figure 9, Compressor Type: Flow Rate vs. Pressure Ratio (Brown, 1997)

The CARIES flow rate requirement of 1.778 SCFM is very low which favors reciprocating and rotary compressors. Along with a low flow rate, the CARIES system requires a very high-pressure output which generates a high-pressure ratio of about 205 (3,014.7 psia/14.7 psia). As seen in the figure above and according to industry standards, the best compressor selection for low flow rates and high-pressure ratios of this magnitude is a multistage reciprocating air compressor.

This selection is further supported by the findings in Section 2. In order to manufacture an air compressor for less than \$2,000, and that can operate for 24 hours per day, it must have a robust design. Reciprocating air compressors have the least intricate designs and are comparatively easier and cheaper to manufacture compared to other types of compressors like screw compressors. As a result, the final product will be of high quality, cheaper, and have lower long-term maintenance costs compared to other types of compressors. In addition, reciprocating compressors are the most common type of compressor found in industry and are regarded as the industry standard (Wildenrad, 2019).

### 3.2.1 Design Choice

Multistage reciprocating compressors can be classified into trunk-piston, which is similar to an automotive piston design, or crosshead type. Trunk-piston designs are

typically more common in small to medium-sized engines and compressors because they are much less susceptible to side thrusts than larger engines and compressors. As a result, trunk-pistons require a less complex and lighter design when compared to crosshead type pistons (Brown, 1997). Based on Atlas Prime's low flow rate requirements, the team decided that a trunk-piston design would work best for their application because the compressor will be relatively small and thus not experience large amounts of side thrust.

Trunk-piston compressors are most commonly found in radial arrangements. These compressors can range anywhere from one to eight cylinders, however, multi-stage arrangements are typically designed in a way that sees piston pairs form a V-shape separated by 90 degrees as seen below in *figure 10* (Brown, 1997). Since this is the industry standard, the team adapted this radial design to the Atlas compressor based on the number of stages it required.

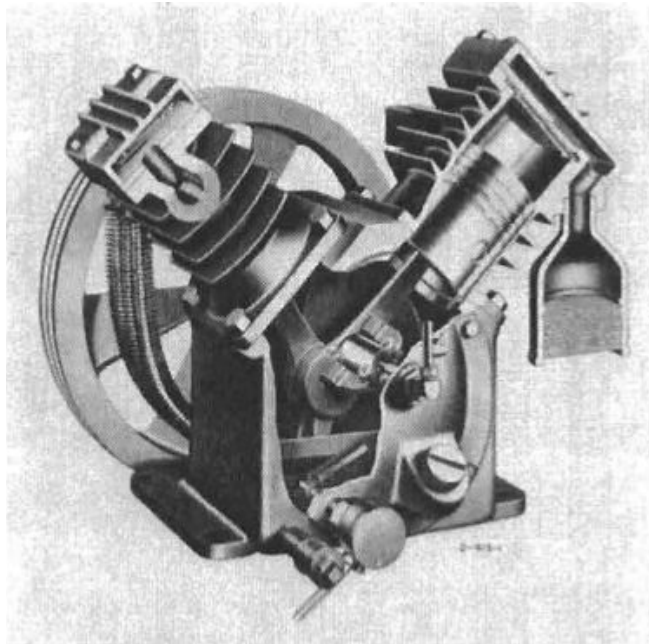


*Figure 10, Trunk-Piston Compressor (Brown, 1997)*

### **3.3 Material selections**

Once the team decided on the type of compressor, the third step was to select the materials out of which to build the major components. The team did this by using CES Edupack to compare different materials against the requirements of the system. Once the team narrowed the search down to three or four potential materials, they created a decision matrix to weigh the most important characteristics and ultimately select the best material for the application.

### 3.3.1 Cylinder Material selection

The team identified several potential cylinder materials. The first step the team took in selecting the material was applying constraints to CES Edupack, shown in *Table 1* below. These constraints were determined based on the load the cylinders would experience during operation and were used to narrow down the potential material options to the most optimal choices.

<b>Price</b>	
By weight	<.50 USD/LB
By volume	< 200USD/ft <sup>3</sup>
<b>Mechanical Properties:</b>	
Young's modulus:	> 20 10 <sup>6</sup> psi
Fatigue Strength at 10 <sup>7</sup> cycles	> 35 ksi
<b>Fracture Properties:</b>	
Fracture toughness:	> 35 ksi.in <sup>.5</sup>
<b>Thermal properties:</b>	
Melting point:	> 800 F
Maximum Service temperature:	> 500 F
Thermal Shock Resistance:	> 350 F

*Table 1, Cylinder Material Properties*

CES Edupack generated a list of materials for the cylinders, and the team selected four based on outstanding qualities such as lowest cost or highest Young's modulus. The list of materials included: AISI 1095, AISI 5140, AISI 4140, and Cast Iron (pearlitic malleable, EN GJMB 650-2).

In order to decide which of the four materials would be best fit for the cylinder, the team created a list of material properties and ranked each property according to its priority: primary, secondary, or tertiary. Primary priority signified that the property was essential to the material choice; for example a high Young's modulus was important due to the loads applied onto the cylinders. Secondary priority signified properties that were ideal

but not the most critical; for example high fracture toughness to mitigate potential crack propagation during operation. Finally, tertiary priority signified properties that could be more flexible and were not vital to operation. This designation applied primarily to manufacturability. While it is an important quality to consider, it is less pertinent to the design process than properties such as fatigue life and endurance limit.

After assigning each property a priority, a weight was assigned on a scale of one to five; one being a low priority and five being a high priority. Using this method aided in the prioritization of properties that are more essential to the compressor's operation.

Property	Priority	Weight (1-5)
High Elasticity Modulus	Primary	5
Low Coefficient of Thermal Expansion	Primary	4
Manufacturability - Malleability - Machinability	Tertiary	1
High Resistance to Thermal Shock	Secondary	2
High Fracture Toughness	Secondary	3
High Fatigue Life	Primary	4
Price	Secondary	3

*Table 2, Weighted Decision Matrix for Cylinder Material*

Using the weights above, the team rated the properties of these materials on a scale of one to five, one being poor and five being optimal. The ratings and the weights were multiplied together to give each material a quality score. All of the materials' quality scores were added together and the material with the highest score was chosen to be the best for the cylinder.

Property	Weight	AISI 1095		AISI 5140		AISI 4140		Cast Iron	
		Rating	Quality	Rating	Quality	Rating	Quality	Rating	Quality
High Young's Modulus	5	4	20	5	25	5	25	3	15
Low Coefficient of Thermal Expansion	4	5	20	4	16	4	16	4	16

Manufacturability - Malleability - Machinability	1	3	3	4	4	4	4	5	5
High Resistance to Thermal Shock	2	4	8	5	10	5	10	3	6
High Fracture Toughness	3	4	12	4	12	5	25	3	9
High Fatigue Life	4	5	20	5	20	4	26	3	12
Inexpensive	3	4	12	4	12	3	9	5	15
<b>Total</b>		<b>91</b>		<b>103</b>		<b>99</b>		<b>82</b>	

*Table 3, Expanded Weighted Decision Matrix for Cylinder Material*

The ratings in the table above were determined by using data provided by CES Edupack. More information about these materials and their properties can be found in *Appendix B: Cylinder Material Properties*. Based on the matrix above, the team determined that AISI 5140 steel would be the best fit for the cylinders. However, it was also determined that an adequate substitute could be found in many steels of a similar composition.

### 3.3.2 Crankshaft, Connecting Rod, and Master Rod Material Selection

The crankshaft, connecting rods, and master rod material must be strong given the forces applied to it during operation. In order to determine the best material, the team used a similar selection process as for the cylinder material.

The first step the team took in selecting the crankshaft material was applying constraints to CES Edupack, shown in *Table 4* below. These constraints were determined based on the loads the crankshaft would experience during operation.

<b>Price</b>	
By weight	<.50 USD/LB
By volume	< 250 USD/ft <sup>3</sup>
<b>Mechanical Properties:</b>	
Young's modulus:	> 30 10 <sup>6</sup> psi
Fatigue Strength at 10 <sup>7</sup> cycles	> 60 ksi

<b>Fracture Properties:</b>	
Fracture toughness:	> 50 ksi.in <sup>.5</sup>

*Table 4, Crankshaft Material Properties*

Using the information above in *Table 4*, CES Edupack generated a list of materials that meet the team's criteria. Three materials were selected: 300M steel, AISI 9260, and AISI 1095. These metals were selected for either having a high fatigue strength, low price per unit volume, or a mixture of both.

After the team established the important material properties, priorities, weights, and ratings were assigned in a similar fashion to the cylinder materials. The matrices are found below. *Table 5* below depicts these priorities and weights.

Property	Priority	Weight (1-5)
High Elasticity modulus	Primary	4
Manufacturability - Malleability - Machinability	Tertiary	1
High fracture toughness	Secondary	3
High fatigue life	Primary	5
Price	Secondary	3

*Table 5, Weighted Decision Matrix for Crankshaft Material*

Using the table above, the team analyzed the material using the material property data in CES Edupack, found in *Appendix C: Crankshaft Material Properties*, to determine the best choice. The same rating process seen in *Section 3.3.1* was used. All of the materials' quality scores were added together and the material with the highest score was used.

Properties	Weight	300M		AISI 9260		AISI 1095	
		Rating	Quality	Rating	Quality	Rating	Quality
High Elasticity modulus	4	5	20	5	20	5	20
Manufacturability - Malleability - Machinability	1	4	4	3	3	2	2

High fracture toughness	3	5	15	3	9	4	12
High fatigue life	5	5	25	4	20	3	15
Inexpensive	3	2	6	4	12	5	15
Total	70		64		64		

*Table 6, Expanded Weighted Decision Matrix for Crankshaft Material*

Based on the matrix above, the team determined that 300M steel would be the best fit for the air compressor's crankshaft. This material was selected because of its high strength mechanical properties despite its high price. Based on these qualifications, 300M steel was also selected for the master rod and connecting rods.

### **3.3.3 Piston Material Selection**

When deciding the best material for the piston heads, a material that was lightweight, easy to machine, and low cost was the primary focus. The team decided it would be most logical to conduct research to find the industry standard for piston material. The most common material for pistons to be made from is aluminum alloys due to their lightweight, high strength, and excellent thermal conductivity (Balu, 2018). The team evaluated several different aluminum alloys to ensure they met their specific requirements and selected aluminum 6061-T6 because of its low cost and accessibility.

## **3.4 Component Selection**

Once the team decided on the materials for the compressor, the fourth step was to select other key components like the valves, motor, and sealing rings. Since there are many types of these components widely available, the team selected the best components based on what was discovered to be the industry standard during their research.

### **3.4.1 Valve Selection**

Valves play an important role in the functioning of an air compressor as they control the flow of air going into and out of the compression cylinders. The team's air compressor features a valve at each inlet and outlet point of the four stages to ensure proper flow throughout the system.

The Stage 1 inlet arrangement is designed to be a suction valve paired with an air filter. The inlet valve will draw air into the compressor that will be compressed through four stages to 3,000 psi. The purpose of the air filter is to filter out any miscellaneous debris which would create wear on the inside of the compressor and shorten its lifespan. In

addition, the filter protects the inlet air from any weather or other small particles and is consistent with most shop air compressors.



*Figure 11, Suction Valve (Discover Valve)*



*Figure 12, Air Compressor Filter (Grainger)*

The Stage 1 outlet valve is designed to be a poppet valve. The team selected this type of valve due to its high flow efficiency. As a result of the air moving very quickly out of stage 1, head losses are amplified exponentially, which makes a  $\frac{3}{8}$ " poppet valve the best option for this cylinder outlet.



*Figure 13, Poppet Valve (McMASTER-CARR)*

The remaining inlet and outlet valves for stages 2, 3, and 4 will be  $\frac{1}{8}$ " ball valves. The team made this decision because stages 2-4 have lower mean exit velocities compared to stage 1. The air also becomes far less viscous during the compression process, further reducing the amount of pressure loss across the valve. Due to this, the team had less of a concern over head loss and opted for a valve that is designed to withstand higher pressures due to its smaller line size. In addition, it proved very difficult to find and obtain  $\frac{1}{8}$ " poppet valves, therefore ball valves are the most economical choice.

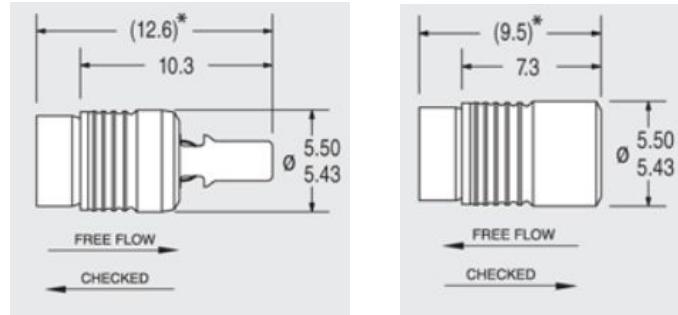


*Figure 14, Drawings of Forward Ball Valve (left) and Reverse Ball Valve (right), (The Lee Company)*

### 3.4.2 Motor Selection

In order to achieve the desired final pressure in this specific arrangement, any selected motor must provide, at bare minimum, 6.3 horsepower at 880 RPM. There are several different types of motors that can be used for this compressor and ultimately is up to Atlas Prime NRG to decide which type of motor they wish to use depending on what is available to them. For the purpose of this design the team fitted the air compressor with a base mounted 7 ½ HP AC motor.



*Figure 15, AC Motor-7 ½ HP (Grainger)*

The motor requires 230 V which will be supplied by the CARIES system and rotates at up to 1,770 RPM. Since the air compressor is designed to run at about 880 RPM, the motor should be paired with a speed reducing gearbox that will decrease the RPM of the motor but maintain its high torque. The gearbox ratio should be 2:1 which will bring the RPM of the system down to about 880 RPM.

### 3.4.3 Bearing and Bushing Selection

Bearings are generally used to reduce friction between parts and enable rotational movement. There are several different types of bearings but the team decided that a combination of ball bearings and bushings would suffice.

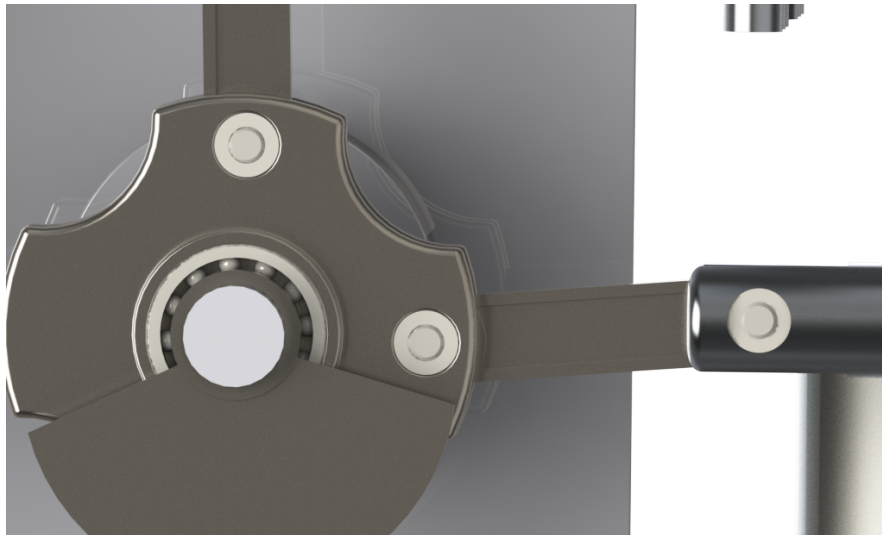


*Figure 16, Bushing and Bearing*

Ball bearings are designed to minimize rotational friction and support radial and axial loads. They are typically used for large rotating elements and do not require lubrication. Due to the size of the air compressor's components, the only component the team decided to use ball bearings for was the crankshaft, as seen above in *figure 16*. The team identified a 35mm ball bearing from McMaster-CARR, seen below in *figure 17*, would fit the needs of the system.



*Figure 17, Ball Bearing-35mm Diameter (McMASTER-CARR)*

Bushings are designed to reduce friction between rotating elements and stationary support members. Their simple, one-piece design allows for them to be manufactured

easily and smaller in size compared to ball bearings, however, they do require some lubrication. The team identified a ½" brass bushing from McMaster-CARR, seen below in *Figure 18*, as the best method for allowing rotational motion at the joints of the crankshaft to the piston rod and the piston rod to the piston. Since bushings require lubrication, they will be lubricated using the system described in *Section 3.4.5*.



*Figure 18, Brass Bushing-½" Diameter (McMASTER-CARR)*

### **3.4.4 Piston Ring Selection**

To achieve maximum efficiency within the compression chambers, it's important to create a perfect seal using piston rings. Piston rings come in many different materials ranging from cast iron, bronze, and stainless steel, however, the team identified PTFE (Teflon) piston rings as the best material for the CARIES air compressor. PTFE piston rings can operate at temperatures up to 500°F and pressures up to 5,800 psi (400 Bar) which falls within the maximum temperatures and pressures that occur within the system.

The benefit of using Teflon piston rings is that they are easy to install and are less likely to twist during installation (Parker, 2018). During the application process, the operator will use pliers or another tool to expand the size of the ring until it is snapped into the groove. In order to make installation easier, it is common to place the PTFE ring in oil or water at 130-140°F for about 5 minutes to soften the material (Hi Tech Seals Inc., 2020). Once the piston rings are in place, a ring compressor is used to ensure the rings are tightly molded to the cylinder head.

In general, PTFE piston rings are very common and can be purchased directly from the manufacturer, like All Seals Inc. Since the compressor the team designed is custom-tailored to the needs of Atlas Prime NRG, the sizing of the cylinders varies from standard sizing. As a result, PTFE piston rings would need to be custom ordered from one of these manufacturers. The diameters of the cylinders the team designed are 85.2 mm, 52 mm, 31.6 mm, and 19.2 mm which fall within the typical range of custom-made PTFE piston rings of 12.7 mm - 2286 mm+ in diameter. As seen below, the pistons have three

grooves for piston rings. The first two grooves are for these PTFE compression rings and the third, wider groove is for an oil wiper ring set.



*Figure 19, Compressor Piston with Grooves for Piston Rings*

### **3.4.5 Oil Lubrication Selection**

There are many pros and cons to designing a lubricated or non-lubricated air compressor. As discovered in Section 2, lubricated compressors are more efficient, cheaper, and more durable compared to non-lubricated compressors in addition to being regarded as the industry standard. These features aligned very well with requirements given to the team by Atlas Prime, ultimately leading the team to decide to proceed with designing a lubricated compressor for the CARIES system.

In order to maximize the efficiency and lifetime of the compressor, it is important to lubricate the internal parts to minimize friction. For a multistage reciprocating compressor, it is the industry standard to use SAE 40 Oil with rust and oxidation inhibitors (Hanlon, 2001). The reason for this viscosity level is due to oil with a higher viscosity reducing flow and subsequently increasing the temperature of bearing surfaces. Oil with a lower viscosity will not provide adequate lubrication (Hanlon, 2001). This type of oil can withstand temperatures of up to 385°F; the maximum temperature the compression chambers reach is 350°F as seen in Chapter 4.

In the main crankcase, the oil reduces friction and carries away heat from the master rod and connecting rod bearings. These bearings traditionally become lubricated through an oil pump with a continuous flow. The compressor piston heads typically

become lubricated via once-through lubrication where the lubricant is supplied to the piston head at a minimal and continuous rate (Mobil, 2019).

In terms of a lubrication system, the team identified an oil dispenser with flow-adjustment valves to be the best solution. An oil dispenser such as McMaster-Carr's Oil Dispenser with Flow-Adjustment Valves, has a 16 oz reservoir that is compatible with SAE 40 Oil and can automatically dispense oil through six different outlets. The flow is controlled by a solenoid and can be adjusted by a valve. The proposed air compressor design has eleven points that would require drip lubrication to ensure proper functioning, thus the system would require two of the oil dispensers described above. In order to transport oil from the dispenser to the lubrication point, a  $\frac{1}{4}$ " hose would be required with a push-to-connect fitting. A diagram of the proposed lubrication system can be seen below.

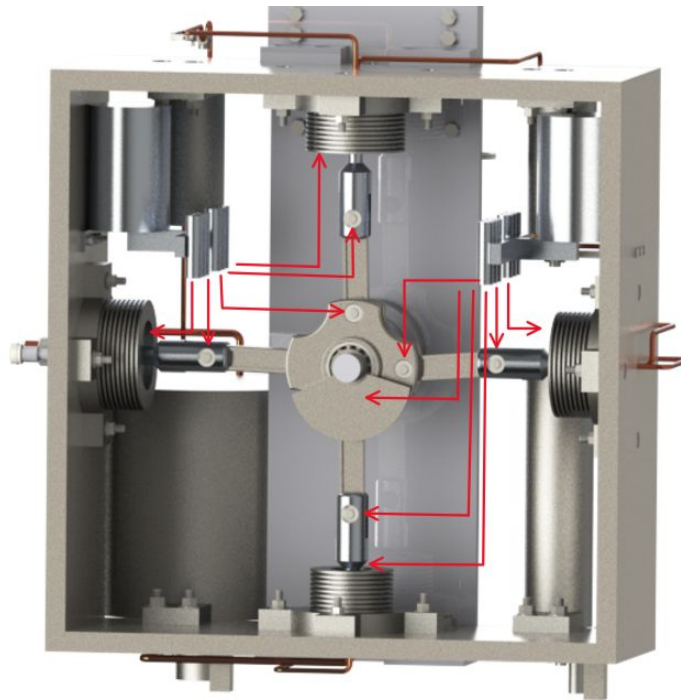


*Figure 20, Lubrication Diagram*

### **3.5 Commercial Alternative Analysis**

To gauge what types of compressors are already available to the market and ensure their designs align with common practices, the team conducted research guided by the requirements given by Atlas Power Systems. This research occurred along with the team's calculations and was valuable because it allowed a modern-day benchmark to be established regarding the mechanical design of the compressor. In addition, the team was able to use this information to brainstorm other creative ideas that would provide

incremental improvements to compressors that were already available. Finally, looking at these commercial alternatives allowed the team to better understand the pricing and manufacturing costs that come along with certain compressor designs and features.

### **3.5.1 “YONG HENG” Paintball Compressor**

Currently, the CARIES prototype system is using the “YONG HENG High Pressure Air Compressor Pump” to do testing for its power system. This compressor is designed to be used for airsoft guns and other light-use applications. In CARIES, the “YONG HENG” compressor can only operate for about fifteen minutes before overheating and shutting off, making it a poor choice for CARIES since this system requires a compressor capable of continuous twenty-four hour operation. The “YONG HENG” Compressor can fill about .25 cubic feet in thirty minutes (.5 per hour) at 4000 psi, and the design requirement is 80 cubic feet at 3,000 psi in forty-five minutes (about 85 cubic feet in an hour) (Amazon, 2019). Even if the “YONG HENG” compressor did not shut off after fifteen minutes, it still would not be able to fill the scuba tanks at the required rate.

### **3.5.2 Scuba Compressors**

The next type of air compressor the team looked into was scuba compressors. The team determined that this would be a good design to look at because the final air is stored in scuba tanks at a similar pressure. Traditionally, scuba compressors follow a 3 or 4 stage oil-lubricated compressor design. In each of the first three stages, air is passed through a compression chamber before passing through an intercooler and going on to the next stage. The final stage of a scuba compressor typically involves a back pressure valve that releases air at around 3,000 psi (AquaViews, 2019). In order to achieve an oil-free output, scuba compressors use a series of filters and moisture separators that remove all traces of oil, carbon monoxide, and any other substances that could potentially be harmful to a diver (AquaViews, 2019).

Overall, this design aligned very closely with the team’s custom compressor. Both had a similar number of stages and compression rates within each stage. After talking to some of the scuba manufacturers, the team determined the price to purchase a basic scuba compressor would be at least \$2,700. This was encouraging as the total manufacturing cost of the ATLAS Prime NRG compressors would be comparable or less in price with significant room to decrease price as production increased.

### **3.5.3 Reciprocating Compressor Disassembly**

Finally, the team looked at a two- stage inline reciprocating compressor provided by Professor Daniello. The team disassembled the compressor in order to see how it was

constructed, identify materials that were used in the design, and to compare that information to their own design. The team was mainly able to gather information about the design of the piston connecting rods, the piston rings themselves, and how the crankshaft was secured and able to freely rotate.

### **Connecting Rods, Piston Heads, and Piston Rings**

Through the deconstruction process, the team gathered valuable information regarding the geometry of the connecting rods. *Figure 21* below depicts the connecting rod on the far right.



*Figure 21, Connecting Rods, Piston Heads, and Piston Rings*

As can be seen, the middle piece of the connecting rod was designed with the structural considerations of an I-Beam. This design choice ensures that the rod is able to be structurally sound and maintain its original shape while the compressor functions. The thickness of the stem and flanges also allows the beam to bend when put under extreme stresses rather than buckle, which can save many of the internal components of the machine barring a severe failure. Additionally, the I-Beam design can maximize the strength of the part while minimizing the amount of materials used. This specific example also shows two cut outs in the center of the beam, which also allow for more weight reduction. This, in turn, reduces the weight of the part as well as the material cost to produce it. Including a lightweight part in the design also benefits the motor selection process, as lighter internal components are much easier to move. By adopting this design, the team can ensure that a strong, optimized, and industry standard component is able to be functional in the final product.

The deconstruction process revealed more information about the connection points of the connecting rod to the piston head. *Figure 22* below shows the internal structure of the piston head.



*Figure 22, Piston Bottom View*

The piston head attaches to the piston rod by sliding over the rod and in between the two extruding geometries inside the piston head. *Figure 23* below also shows the side view of the piston in order to see the exact intersection of the piston head and rod.

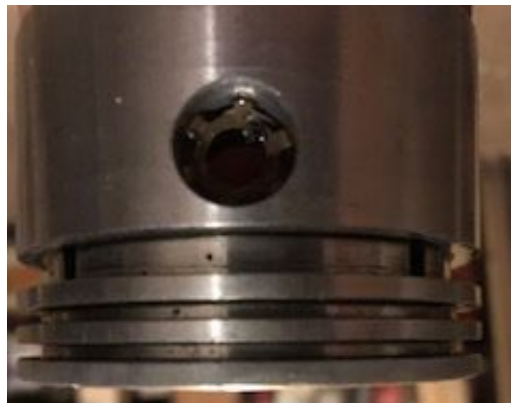


*Figure 23, Piston Side View*

The above image shows a hole in the side of the piston where a metal dowel is typically inserted in order to attach the two components. Additionally, clips are placed on either end of this passage to keep the metal dowel from coming loose and falling out of its resting place between the piston head and rod.

From these observations, it was determined that the team's compressor design would need to mimic these in some way. The connection point of the piston head and rod ensures a strong bond between these two different components, as the internal geometries

of the piston head eliminate any lateral motion of the piston head and connecting rod during operation. This will put less stress on the connecting metal dowel pin, and provide a reliable and strong joint. Finally, while the star clips shown in *Figure 23* are not the exact ones that need to be used, some form of fastener is required.

The addition of piston rings was another design aspect that was improved by the deconstruction of this compressor. *Figure 23* above shows the three grooves that need to be cut into the piston head in order to place the rings themselves. The first two grooves are of similar size, while the third is larger. Additionally, *Figure 24* below shows the fully assembled piston head.



*Figure 24, Piston Ring Assembly*

Examining these different components allowed for the sizing of the piston rings to be done properly. The top two rings maintain a loose fit in the groove they are placed in. This showed that these rings when fully compressed in the chamber needed to have a slightly larger diameter than the piston head itself, but maintain a loose fit on the piston head in order to more easily conform to the shape of the chamber. Additionally, a looser fit allows for easier placement and removal of the rings during maintenance. Finally, the bottom ring was observed to have a much tighter fit around the piston head. This is most likely due to the fact that the oil removed from the chamber by the top two rings needs to enter the holes present in this larger ring to be returned to the lubrication system. Observation of these components will help determine the proper design and tolerancing of the piston heads in the team's compressor.

## Crankshaft

The deconstruction also allowed for the informed design of the crankshaft. *Figure 25* below depicts the crankshaft.



*Figure 25, Crankshaft Assembly*

As shown above, the crankshaft is secured at both ends by press-fit ball bearings. These ball bearings are then held in place by divets and cut-outs in the case surrounding all of the internal components. By performing this analysis, a protocol to firmly secure the crankshaft will be able to be determined, as well as the hardware necessary to ensure that the component is able to stay in a single position, while also rotating freely during operation.

## Chapter 4 - Methodology and Calculations

After selecting the compressor type, arrangement, the thermodynamic and physical qualities of the air, compression chambers, and cooling mechanisms had to be calculated and sized to ensure the compressor met the CARIES system requirements. In the following sections the assumptions, calculations, and discussions for the compression chamber sizing, intercoolers, and post-compression water disposal methods are presented. Estimations of the overall efficiency are provided at the end with a discussion on the different methods of calculation.

### 4.1 Assumptions

For the calculations below the following set of assumptions were put in place. The system was assumed to be working at steady state conditions, compression was assumed to be polytropic, the compressibility factor of air was assumed to be approximately 1 for all inlets and outlets, and the cylinder material was assumed to be isotropic. When calculating values for the intercoolers the water was assumed to enter the system at ambient temperature, and there was assumed to be no stray heat transfer to the surroundings. In reality, many of these assumptions are variable. However, the team determined the system would be operating at conditions approximate enough to the assumptions, and as a result, the variation would not significantly affect performance.

### 4.2 Initial Sizing from Volumetric Efficiency

The sizing process began with an examination of the cylinder dimensions required to achieve the desired exit pressure at each stage. To proceed with the discussion two concepts need to be introduced: piston displacement and inlet capacity. Piston displacement is the volume of air measured at standard temperature and pressure (STP) displaced per minute by the movement of the piston. Inlet capacity is the amount of air that can be compressed by the piston and cylinder given a certain volumetric flow rate and compression ratio (Brown, 1997).

Understanding these concepts, the following equations were used to determine the realistic volumetric efficiency and inlet capacity of each cylinder. All equations are from Brown 1997.

$$Piston\ Displacement = Stroke * RPM * \pi * (Internal\ Radius)^2$$

$$Realistic\ Volumetric\ Efficiency = 0.97 - [(\frac{1}{r}) * r_p^{\frac{1}{k}} - 1] * c + L$$

$$Inlet\ Capacity = Piston\ Displacement * Realistic\ Volumetric\ Efficiency$$

*Figure 26, Volumetric Sizing Equations (Brown, 1997)*

Variable  $f$  stands for the ratio of the outlet compressibility to the inlet compressibility,  $r_p$  is the ratio of outlet pressure to inlet pressure, and variable  $L$  is a modifier based on the oil in the compressor. Oiled compressors are given an  $L$  value of 0.04 and non-oiled compressors are given an  $L$  value of 0.07. The variable  $c$  found in the volumetric efficiency equation stands for percent clearance: the additional volume of air that is re-expanded to inlet pressure after the discharge valve is closed (Brown, 1997). In the image below, the clearance volume is the volume between the piston head and the dashed line.



*Figure 27, Clearance Visualization (Brown, 1997)*

The calculations were iterated from 0% to 20% clearance for each cylinder. The selection was determined by relative cylinder size and volumetric efficiency. It was determined that any volumetric efficiency below 70% was unacceptable; rule of thumb for combustion engine piston cylinder sizing confirms that any clearance percentage above 10% is unacceptable. Therefore the selection for the first and largest cylinder gives a realistic volumetric efficiency of 72.7%. The clearance percentage then went down by 2% for every subsequent cylinder.

From these calculations, the team was able to determine the required volume in each cylinder. The team opted to use a small stroke of 15 millimeters so that each piston rod was of a length where buckling was not a concern. Based on the ratio of outlet density to inlet density, a height and internal radius was found for each cylinder.

#### **4.2.1 Calculating Cylinder Stresses from a Thick-Walled Model**

Cylinder stresses were calculated using the thick-walled pressure vessel model as seen in Ugural and Fenster (2012). Having calculated the necessary volume in the cylinder to intake the desired amount of air, the team was able to iterate independent variable wall thickness for each cylinder in order to determine radial and hoop stresses from the equations seen below.

$$\sigma_r = \frac{r_i^2 P_i - r_o^2 P_o}{(r_o^2 - r_i^2)} - \frac{(P_i - P_o) r_i^2 r_o^2}{(r_o^2 - r_i^2) r^2}$$

Figure 28, Radial Stress in the Cylinders as a Function of Radii and Pressures

$$\sigma_\theta = \frac{r_i^2 P_i - r_o^2 P_o}{(r_o^2 - r_i^2)} + \frac{(P_i - P_o) r_i^2 r_o^2}{(r_o^2 - r_i^2) r^2}$$

Figure 29, Hoop Stress in the Cylinders as a Function of Radii and Pressures

$P_i$  stands for internal pressure,  $P_o$  for external (atmospheric) pressure,  $r_i$  for internal radius, and  $r_o$  for external radius. After calculating the stresses in each configuration of wall thickness, cylinder dimensions were selected based on the criteria of hoop stress magnitude and material cost. Each cylinder was given dimensions which brought the hoop stress to a magnitude below the fatigue limit of the material while providing minimal material cost to the manufacturer. Internal radius decreases as the stages progress, keeping within industry standards for a multi-stage reciprocating compressor.

#### 4.2.2 Cooling

As with many energy systems, the compressor required cooling for the working fluid. However, the unique challenge was presented by having only ambient temperature water for cooling in addition to a low air flow rate. The former means that the lowest available temperature for the coolant, and thus the air, was 303 degrees Kelvin. The latter means that the required dimensions of these heat exchangers are larger than average for compressors with these output requirements. Due to this constraint, all air-side arrangements, minus the aftercooler, are coiled in order to provide the maximum heat transfer area per unit volume of heat exchanger. From thermodynamics, the compression ratio, and thus number of stages, was dictated by the maximum operating temperature in the compressor. Setting a maximum operating temperature of 450 Kelvin (Bloch, 2006), the maximum temperature difference across each stage is 147 Kelvin. From  $Q = \frac{dm}{dt} \cdot C_p \cdot \Delta T$ , it was calculated that each intercooler needed to dissipate approximately 0.22 kW of heat from the air.

The design choice for all cooling devices is a counter-flow concentric tube heat exchanger. For our given operating parameters, this arrangement provided the most effective cooling for the lowest material price. This arrangement is realized by flowing the air through small diameter copper tubes between compression stages and flowing water in the antiparallel direction in a larger diameter aluminum tube concentric with the copper

pipng. Compact cross-flow exchangers were considered, however, both the manufacturability and price thereof are well beyond the budget of the project.

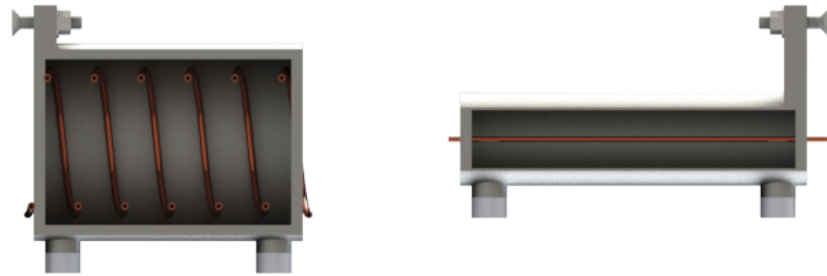


Figure 30, Cross Section of Heat Exchangers at Stage 1 exit (left) and Stage 4 exit (right)

Determining the size of each exchanger was accomplished by means of employing a heat resistance analogy  $\frac{1}{U} = \frac{1}{h_{air}} + \frac{1}{h_{water}}$ .  $U$  is the overall heat exchanger coefficient,  $h_{air}$  is the air-side convection coefficient, and  $h_{water}$  is the water-side convection coefficient. It is assumed that the internal piping provides minimal conductive resistance to the heat transfer, and the thickness of the piping does not change the available surface area significantly from inside to outside. In order to tabulate the convection coefficients, calculations for the friction factors ( $f$ ), Reynolds numbers ( $Re$ ), and subsequent Nusselt numbers ( $Nu$ ) were iterated with copper tube diameter as the independent variable. The aftercooler and all intercoolers except for the device between stages 1 and 2 used the following correlation for Nusselt number obtained from Bergman et al. (2011):  $Nu = 0.023 * Re^{0.8} * Pr^{0.3}$ .  $Pr$  is the Prandtl number for each material at a temperature halfway between the entry and exit temperatures. The intercooler between stages 1 and 2 did not have supply air which could reach fully turbulent Reynolds numbers and thus used the following correlation from the same source.

$$Nu_D = \frac{(f/8)(Re_D - 1000)Pr}{1 + 12.7(f/8)^{1/2}(Pr^{2/3} - 1)}$$

Figure 31, Nusselt Number Correlation for First Cooling Device (2011)

The results of the sizing are provided below.

Stages	Heat Rejected (kW)	Aluminum Shell Diameter (in)	Copper Tubing Diameter (in)	Number of Coils	Coil Radius (in)	Effective Length of Tubing (m)
1 - Exit 2-Entry	0.22	12	5/16	8	5.71	7.28

2 - Exit 3 - Entry	0.22	3	1/8	5	1.22	0.965
3 - Exit 4 - Entry	0.23	3	1/8	5	1.22	0.965
4 - Exit	0.18	3	1/8	0	-	0.252

*Table 7, Heat Exchanger Parameters*

The only stage which did not require the use of coils to attain reasonable dimensions is stage 4. The material properties and velocity of the air sufficiently increase the convection coefficient inside the tubes to the point that the needed length is reasonable in comparison to the overall dimensions of the compressor.

A problem arises in the cooling devices regarding the condensation of humidity while the air is being cooled. Given the altered conditions of the flow after each stage, water will condense inside the cooling devices. This mainly presents a problem in stage one, and in solution we have installed a drain leg connected to the air tubing at the bottom of the loops to provide a path to the outside for the water.

### 4.2.3 Motor Specifications from Torque

In order to select an appropriately-sized motor, the team had to first calculate the torque each compression stage provided during operation. The derivation can be found in the Appendix. Each stage's torque was calculated individually as a function of crank angle and then summed for each crank angle. The superposition of the torques is presented on the graph below.

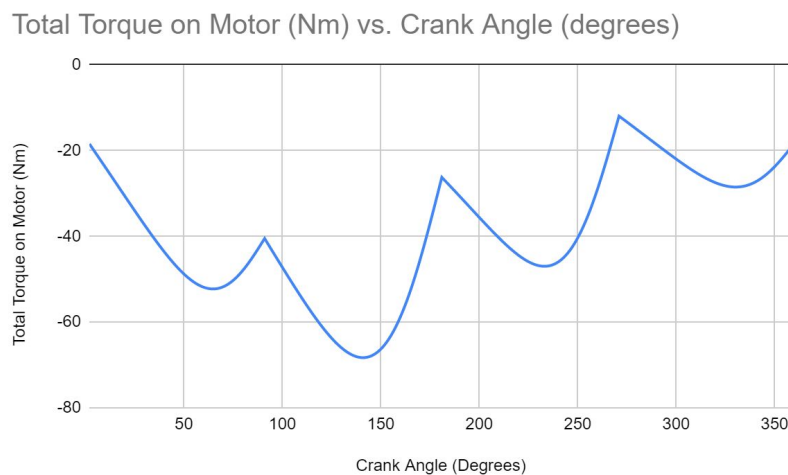


*Figure 32, Torque on Motor vs Crank Angle*

The largest magnitude torque experienced by the motor is 68 Newton-meters occurring at a crank angle of around 150 degrees from the equilibrium axis. From this it was determined that the motor needed to be specified for 6.3 horsepower or greater.

#### 4.2.4 Overall Efficiency

The current configuration is 34.9% efficient. This number comes from summing the ideal minimum required power for each stage and dividing by the power input from the motor. The equation used to calculate each stage's efficiency is:

$$Power = Inlet\ Pressure * Inlet\ Volumetric\ Flow\ Rate * \frac{k}{k-1} * (r_p^{\frac{k-1}{k}} - 1).$$

*Figure 33: Theoretical Power per Stage (Brown, 1997)*

From this, the team determined a minimum power of 1.7 kW is needed for the operational requirements. The motor required to run this arrangement must provide, at minimum, 4.7 kW due to the torque loadings from the cylinders.

Further design iterations could increase compressor efficiency. Areas to explore include: RPM reduction, shorter strokes, and outsourcing to professional compressor design companies. There are most certainly other areas not shown here which could improve the performance. The team recommends following up on this design with a compressor manufacturer in order to review and validate the design.

## Chapter 5 - CAD

The main deliverable of this project was a design of an air compressor for the CARIES system. The team created a Solidworks model of the air compressor to be given to Atlas Prime. This model allows Atlas Prime to understand the size and weight of the air compressor and can help with planning logistics. *Figure 34* below shows a rendering of the final design. See *Appendix D* for renderings of key components.

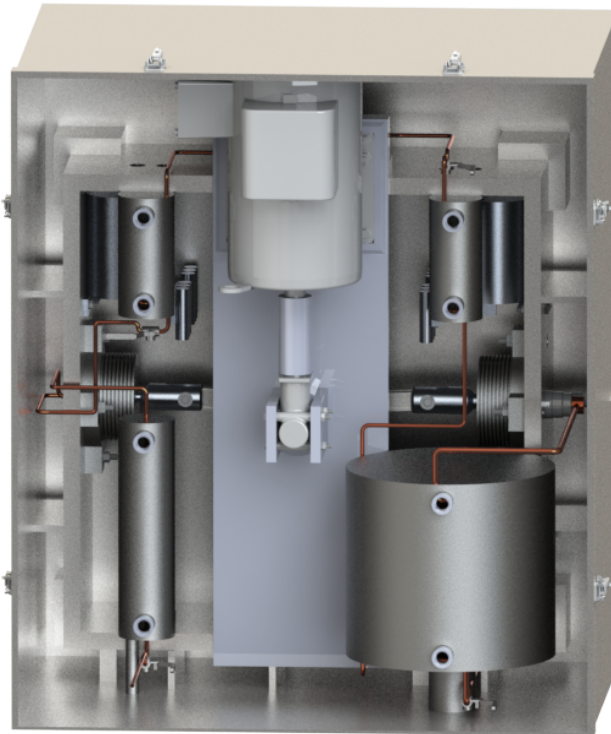


*Figure 34, Air Compressor Rendering*

The air compressor is intended to be easily manufactured on a small scale, and the design can be easily modified for large-scale production as the company grows. Additionally, the design allows for easy assembly and repair of the compressor..

*Figure 35* below shows a cross-sectional view of all four stages. The radial and reciprocating aspects of the compressors are demonstrated by the positions of the pistons and cylinders.

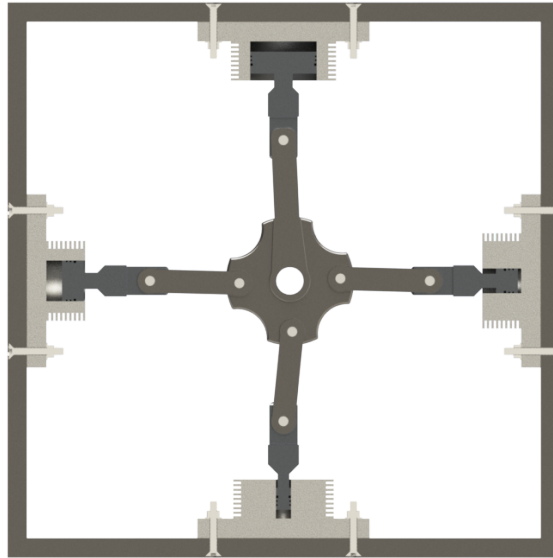


*Figure 35, Cross-Sectional View*

*Figure 36* below shows a front and angled view of the compressor casing. The front piece of the case has eight openings for hoses running water to cool the air in the heat exchangers. All the hose openings have covers to prevent debris from entering the case. In the image on the right, the suction valve is represented by a small slot. The front and back of the case are held together using six draw latches for easy internal access.

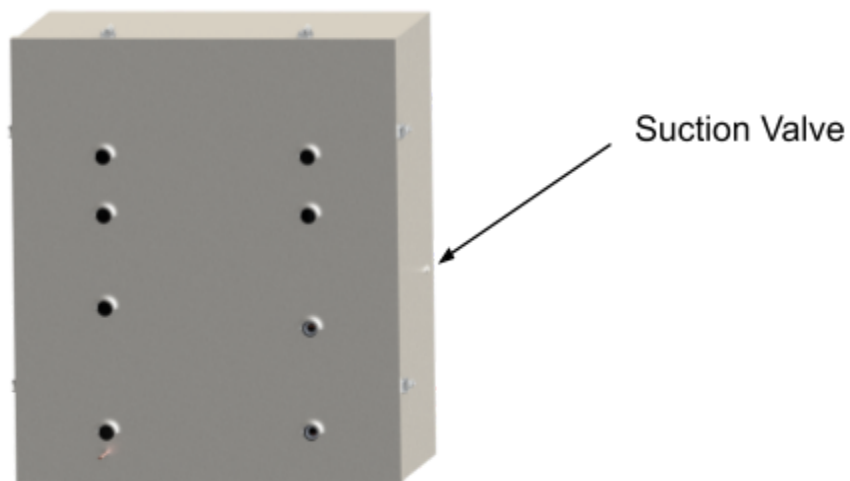


*Figure 36, Compressor Casing*

*Figure 35* below shows the major offset rotation pin. This offset pin goes through the center of the crankshaft and master rod and allows the piston to oscillate. The pin is radially offset 7.5 mm to produce a 15 mm stroke. The right side of the pin is intended to

connect to a gearbox and/or motor to initiate the rotation. The inside of the right side of the pin is hollowed out to be the negative of the shaft of the gearbox or motor. The gearbox or motor has a notch in the shaft resulting in locked rotation of the major offset pin. The center of the pin is wider to keep the pin centered along the back of the frame of the compressor, the pin must stay centered as that is what creates the 15 mm stock and moves the piston a proper distance. Finally, the left side holds the crankshaft and counterweight, not visible in this figure. The crankshaft is free moving, not rotating, so it will move to create a stroke but it will not rotate. The counterweight is also not attached to this pin and is free rotation because it swings with the air compressor to absorb vibrations.



*Figure 37, Major Offset Rotational Pin*

Below, *Figure 38* shows the different heat exchanger designs. The intercoolers after compressor stages one, two, and three use the design on the left. The use of a coil design helps save volume while maximizing the effective cooling area. The heat exchanger design on the right is used to cool the air after stage four compression. A much smaller length of the airline needs to be cooled, therefore a straight pipe is used with a smaller diameter water jacket to reduce material and manufacturing cost.

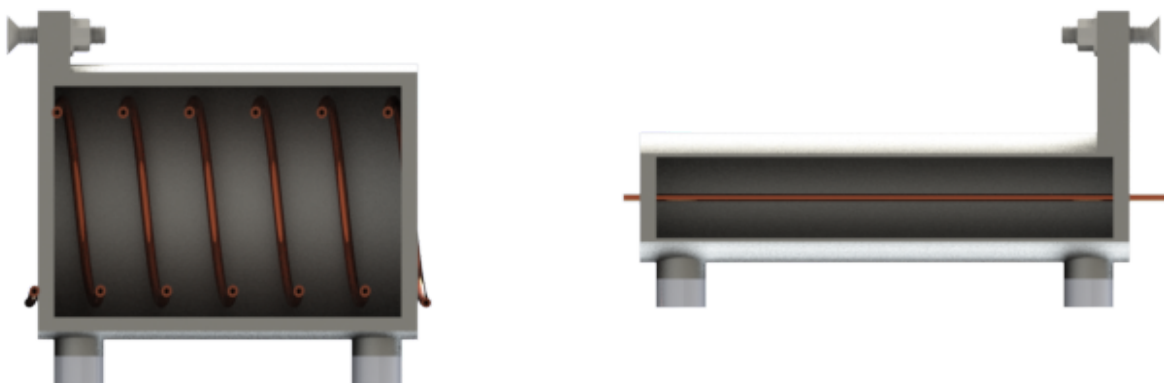


*Figure 38, Heat Exchanger Cross-sectional View*

*Figure 39* below shows a back view of the air compressor where the heat exchangers are located. The copper pipes show the path the compressed air travels: going from cylinder, to heat exchanger, and then into the next cylinder. The stage one cooling device can be seen in the bottom right corner with a larger diameter coil. Stage two and three are located on the top also using a coil design, but with smaller radii resulting in a smaller water jacket. Stage four can be seen in the bottom left corner; it is longer as the airline does not use a coil design.

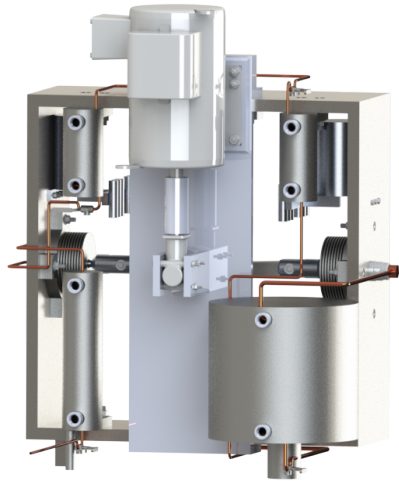


*Figure 39, Heat Exchanger System*

## Chapter 6 - Failure Analysis (ANSYS)

To ensure the team's air compressor design was robust and properly constructed, the team conducted several failure tests of the Solidworks model through ANSYS Workbench Simulation Software. These simulations involved investigating applied forces and pressures on the cylinders, pistons, and connecting rods in order to ensure that excessive amounts of deformation were not occurring. The tables below show the amount of deformation and stress each part experiences based on the applied load.

<b>Cylinder Load from Maximum Pressure in Chamber Ansys Simulation Results</b>			
<b>Stage</b>	<b>Applied Load (kPa)</b>	<b>Maximum Deformation (m)</b>	<b>Maximum Stress (Pa)</b>
1	404	$2.6657 \times 10^{-7}$	$1.2902 \times 10^6$
2	1616	$4.7177 \times 10^{-7}$	$4.1026 \times 10^6$
3	6464	$8.1972 \times 10^{-7}$	$1.1947 \times 10^7$
4	20788	$1.4291 \times 10^{-6}$	$4.1476 \times 10^7$

*Table 8, Cylinder Load from Maximum Pressure in Chamber Ansys Simulation Results*

<b>Piston Load from Maximum Pressure in Chamber Ansys Simulation Results</b>			
<b>Stage</b>	<b>Applied Load (kPa)</b>	<b>Maximum Deformation (m)</b>	<b>Maximum Stress (Pa)</b>
1	404	$1.1337 \times 10^{-5}$	$1.3929 \times 10^7$
2	1616	$1.7713 \times 10^{-5}$	$6.7371 \times 10^7$
3	6464	$2.5201 \times 10^{-5}$	$3.9948 \times 10^7$
4	20788	$3.9751 \times 10^{-5}$	$9.8140 \times 10^7$

*Table 9, Piston Load from Maximum Pressure in Chamber Ansys Simulation Results*

<b>Connecting Road Load From Piston Head Ansys Simulation Results</b>				
<b>Stage</b>	<b>Applied Load X (kPa)</b>	<b>Applied Load Y (kPa)</b>	<b>Maximum Deformation (m)</b>	<b>Maximum Stress (Pa)</b>
1	21	403	$9.7426 \times 10^{-6}$	$3.8073 \times 10^6$
2	85	1614	$9.9859 \times 10^{-6}$	$7.1570 \times 10^6$

3	338	6455	$3.9944 \times 10^{-5}$	$2.8628 \times 10^7$
4	1088	20760	$9.8135 \times 10^{-5}$	$8.0024 \times 10^7$

*Table 10, Connecting Rod Load From Piston Head Ansys Simulation Results*

<b>Connecting Rod Perpendicular Load Ansys Simulation Results</b>			
<b>Stage</b>	<b>Applied Load (kPa)</b>	<b>Maximum Deformation (m)</b>	<b>Maximum Stress (Pa)</b>
1	404	$1.3365 \times 10^{-6}$	$5.3555 \times 10^6$
2	1616	$3.7377 \times 10^{-6}$	$1.1982 \times 10^7$
3	6464	$1.4951 \times 10^{-5}$	$4.7927 \times 10^7$
4	20788	$4.8081 \times 10^{-5}$	$1.5413 \times 10^8$

*Table 11, Connecting Rod Perpendicular Load Ansys Simulation Results*

Running these simulations revealed the maximum deformations and stresses that would be experienced by numerous components in each stage. All observed maximum deformations are considered negligible, and no noticeable deformation should occur. Stresses are well within the allowable amount for both the steel and aluminum used to manufacture these parts.

## Chapter 7 - Results

This section contains an overview on the Bill of Materials, design changes and recommendations, and potential commercial compressor alternatives. The bill of materials goes over an overview of commercial parts the team recommends for the compressor along with raw material costs. Recommendations give suggestions that ATLAS Prime can choose as their product grows with time. Finally, given the air compressor is just one part of the CARIES system, the team has given commercial options for testing while other parts of the system are being developed.

### 7.1 Cost Analysis

The team has constructed a Bill of Materials, quantity, and total cost based on different items used for the construction of the air compressor below in *Table 12*:

Item	Quantity	Unit cost	Total cost
Dowel Pins	7	\$1.16	<b>\$8.16</b>
Ball Bearings	2	\$13.95	<b>\$27.90</b>
High-Load Oil-Embedded SAE 863 Bronze Sleeve Bearing (Bushings)	14	\$0.82	<b>\$11.48</b>
558 SERIES CHECK VALVE – FORWARD FLOW (ball valves)	3	\$15	<b>\$45.00</b>
558 SERIES CHECK VALVE – REVERSE FLOW (ball valves)	3	\$15	<b>\$45.00</b>
Brass Threaded Check Valve (poppet valve)	1	\$39.15	<b>\$39.15</b>
Brass Threaded Check Valve (suction valve)	1	\$36.96	<b>\$36.96</b>
Oil Dispenser with Flow-Adjustment Valves	2	\$352.74	<b>\$705.48</b>
Draw Latches with Safety Catch	6	\$7.20	<b>\$43.20</b>
Air Compressor Filter/Silencer	1	\$15.90	<b>\$15.90</b>
Black-Oxide Alloy Steel Hex Drive Flat Head Screw	16	\$1.24	<b>\$19.84</b>
High-Strength Class 10 Steel Flange Nut	16	\$0.18	<b>\$2.86</b>

Black-Oxide Alloy Steel Hex Drive Flat Head Screw	16	\$1.16	<b>\$18.56</b>
High-Strength Class 10 Steel Flange Nut	16	\$0.30	<b>\$4.82</b>
High Pressure Copper Tubing	30 ft	\$2.00	<b>\$60.00</b>
4.5 in Diameter Low-Carbon Steel Rod	1 ft	\$168.93	<b>\$168.93</b>
1.75 in thick, 1.75 in width Low-Carbon Steel Bar	1 ft	\$42.16	<b>\$42.16</b>
3.5 in Diameter Aluminum Rod	1 ft	\$63.85	<b>\$63.85</b>
2.25 in Diameter Aluminum Rod	1 ft	\$26.45	<b>\$26.45</b>
1.75 in Diameter Aluminum Rod	2 ft	\$34.24	<b>\$34.24</b>
1 in thick, 10 in width Low-Carbon Steel Sheet	4 ft	\$432.92	<b>\$432.92</b>
2 in thick, 8 in width Low Carbon Steel Bar	1 ft	\$216.77	<b>\$216.77</b>
4 in Diameter Low-Carbon Steel Rod	1 ft	\$130.73	<b>\$130.73</b>
<b>Total</b>			<b>\$2200.36</b>

*Table 12, Parts Quantity and Cost List*

The Bill of Materials was given to Atlas Prime NRG to help with the production of the air compressor. The list provided to ATLAS Prime NRG list; quantity, size, and specification of these items. Items were recognized as essential and replaceable based on whether the part could easily be switched out for a similar component or not. Parts that could be switched for a similar component were provided with a viable supplier however because items such as a screw are offered from many different companies we have allowed Atlas Prime NRG to decide whether they would like to use the company recommended or a different company. Essential part should not be switched out for different components without a proper analysis, this is because components such as valves affect efficacy of the design of the compress

The table above does not include a motor or gearbox. Section 3.4.2 provided the team's suggestion for motor selection based on their calculated motor requirements. Using these motor requirements Atlas Prime NRG can configure their own motor and decide whether or not they would like to use a gearbox.

## **7.2 Recommendations**

The current design of the piston air compressor is suitable for small-scale production with limited access to manufacturing equipment. Design changes can be made to the product as production increases, to decrease manufacturing costs and time. Additional compressor changes are discussed in section 7.2.1 and 7.2.2 below.

### **7.2.1 Design Changes**

Future designs could choose to use a thinner outer frame to reduce the amount of material being used, resulting in a lower material cost and lighter weight structure. Vibration and stress analyses should be done before design changes are made to the frame to ensure failure will not occur during operation.

In addition, material changes could be made to parts like the major offset rotation pin. Many features of the air compressor are currently designed to be constructed out of steel due to its relatively low cost. A more in-depth analysis of the pros and cons of potential materials could reveal a more optimal choice, however steel will satisfy all of the engineering and financial needs of the customer. Optimizing the compressor's materials will help improve performance, cost, and manufacturability.

### **7.2.2 Bushing and Ball Bearings**

As the rate of production of ATLAS Prime NRG's air compressor increases, it is recommended that the bushing that connects the piston to the piston rod and the piston rod to the crankshaft are changed out for ball bearings. Ball bearings do not need to be lubricated so this would eliminate eleven lubrication points and only the four cylinders would need to be lubricated. Many elements were designed to be lightweight by reducing the overall dimensions. The current design of the piston and piston arm cannot support a ball bearing. Design changes would need to be made to accommodate ball bearings on these elements but can result in benefiting the overall compressor.

## **7.3 Commercial Alternatives**

In the event that Atlas Prime NRG falls under a time constraint, needs an emergency air compressor, or experiences delays while manufacturing the air compressor designed by the team, the following commercially made air compressors can be used as a replacement. According to the manufacturers, all of the following compressors can meet Atlas Prime NRG's pressure and flow requirements. All three compressors are designed for scuba use which means they are rated for Grade E air quality which will not damage the CARIES air storage tanks.

The first compressor is the Coltri MCH13 Compact Evo Compressor. The cost of this compressor is set at \$11,000 and has a maximum operating pressure of 5,000 psi at 7 CFM. This system is designed to last for over 10 years with long usage times like the CARIES system will operate.



*Figure 40, Nuvair Coltri MCH13 Compact Evo Compressor (Nuvair, 2019)*

The second compressor is the 9HP Scuba High-Pressure Air Compressor. The cost of this compressor is \$6,000 for one or about \$4,800 each if five are bought at a time. The maximum operating pressure of this compressor is 4,500 psi at 9.5 CFM.



*Figure 41, Toolots Scuba High Pressure Air Compressor (Toolots, 2019)*

The third compressor is the Coltri MCH6/3E . The cost of this compressor is set at \$3,000 and has a maximum operating pressure of 4,500 psi at 2.8 CFM.



*Figure 42, Nuvair COLTRI MCH6 Portable High Pressure Compressor (Nuvair, 2019)*

While these options are above ATLAS Prime NRG's budget, they offer the benefit of being proven technology. In order to determine the best direction for the CARIES project, ATLAS Prime NRG will need to consider the projected timing of prototyping, design changes, and manufacturing of a compressor which these options will not require.

## References

- Air Compressors Direct. (2019). *Rotary Screw Air Compressors*. Retrieved from <https://www.aircompressorsdirect.com/tools/rotary-screw-air-compressors.html>
- Air Compressor Talk. (2019). *What Type of Work Can Be Done by an Air Compressor?*. Retrieved from <https://www.aircompressortalk.com/type-work-can-done-air-compressor/>.
- Almasi, A. (2014, May 6). *The pros and cons of axial compressors*. Retrieved from <https://www.plantservices.com/articles/2014/the-pros-and-cons-of-axial-compressors/>.
- Amazon. (2019). *YONG HENG High Pressure Air Compressor Pump, Auto-Stop 110V 30Mpa Electric Air Pump Air Rifle PCP 4500PSI Paintball Fill Station for Fire Fighting and Diving*. Retrieved from <https://www.amazon.com/Pressure-Compressor-Auto-Stop-Electric-Paintball/dp/B07RWZB52G>.
- AquaViews. (2019, January 4). *A Complete Guide For Scuba Compressors - AquaViews - Leisure Pro*. Retrieved from <https://www.leisurepro.com/blog/scuba-gear/complete-buying-guide-scuba-compressors/>.
- Arfalk, E. (2014, February 27). *How it Works: Piston Compressor*. Retrieved from <https://www.thecompressedairblog.com/how-it-works-piston-compressor>.
- AshAir. (2019, July 31). *What are the advantages of using a Rotary Screw Compressor?* Retrieved from <https://www.ashair.co.nz/blog/advantages-of-rotary-screw-compressors>.
- Atlas Copco. (2019). *Who does a screw compressor work?*. Retrieved from <https://www.atlascopco.com/en-au/compressors/air-compressor/screw-compressor-technology-explained>
- Atlas Prime NRG. (2019). *CARIES*. Retrieved from <https://www.atlasprimenrg.com/caries>
- Atula, H. (n.d.). *Dau may nen khi truc vi*. Photograph.
- Balu, S. (2018, November 12). *Reciprocating Air Compressors Explained*. Retrieved from <https://www.brighthubengineering.com/hvac/68218-about-reciprocating-air-compressors-explained-ii/>

- Beckett, G. (2019, October 27). *Routine blackouts in Haiti symbolize a loss of political power for its citizens*. Retrieved from <https://theconversation.com/routine-blackouts-in-haiti-symbolize-a-loss-of-political-power-for-its-citizens-110950>
- Bergman, T., Lavine, A., Incropera, F., DeWitt, D. (2011). *Fundamentals of Heat and Mass Transfer: Fifth Edition*. John Wiley & Sons Inc.
- Bloch, H.P. (2006). *Compressors and Modern Process Applications*. John Wiley & Sons Inc.
- Boyce, M. P. (2012). *Gas turbine engineering handbook*. Waltham, MA: Butterworth-Heinemann is an imprint of Elsevier. doi: <https://doi.org/10.1016/C2009-0-64242-2>
- Brown, R. N. (1997). *Compressors: Selection and Sizing Second Edition*. Gulf Professional Publishing.
- CompressorWise. (2019). *Rotary Screw Compressor Tips*. Retrieved from <http://www.compressorwise.com/reports/RotaryScrewTips.html>.
- Dugan, T. (n.d.). *Centrifugal Air Compressor Controls and Sizing Basics*. Retrieved from <https://www.airbestpractices.com/technology/air-compressors/centrifugal-air-compressor-controls-and-sizing-basics>.
- Dunning, D. (2017, April 24). *Advantages & Disadvantages of Rotary Screw Air Compressors*. Retrieved from <https://sciencing.com/advantages-rotary-screw-air-compressors-7808180.html>.
- Ebrahimi, M. (2019). *Disadvantages and advantages of compressors Screw (spiral) to piston compressors (went and return)*. Retrieved from [http://behsanair.com/en/shownews/1011/Disadvantages-and-advantages-of-compressors-Screw-\(spiral\)-to-piston-compressors-\(went-and-return\)](http://behsanair.com/en/shownews/1011/Disadvantages-and-advantages-of-compressors-Screw-(spiral)-to-piston-compressors-(went-and-return)).
- export.gov. (2019, August 2). *Haiti - Energy*. Retrieved from <https://www.export.gov/apex/article2?id=Haiti-Energy>
- Frey, M. (n.d.). *Inline 6 Cylinder with firing order 1-5-3-6-2-4*. Photograph.
- FS-Elliott. (n.d.). *How Does a Centrifugal Compressor Work?* Retrieved from <https://www.fs-elliott.com/how-does-a-centrifugal-compressor-work>.

- Gardner Denver. (2019). *Rotary Screw compressors*. Retrieved from <https://www.gardnerdenver.com/en-us/knowledge-hub/articles/screw-compressors>.
- Hanlon, P. C. (2001). *Compressor handbook*. New York: McGraw-Hill.
- Hi Tech Seals Inc. (2020, February). *Installation of PTFE Teflon Piston Seals*. Retrieved from <http://www.hitechseals.com/index.asp?lang=>
- Ingersoll Rand. (n.d.). *The Advantages of Centrifugal Compressor Technology*. Retrieved from <https://www.ingersollrandproducts.com/content/dam/ir-products/Compressors/products/Advantages of Centrifugal Compressor Technology.pdf>.
- Mannan, S. (2012). *Lees loss prevention in the process industries: hazard identification, assessment and control*. Amsterdam: Elsevier Butterworth-Heinemann. doi: <https://doi.org/10.1016/C2009-0-24104-3>
- mech4study. (2019, July 21). *Mechanical Engineering Blog*. Retrieved from <https://www.mech4study.com/>.
- Mechanical Engineering Site. (2017, April 14). *Centrifugal Compressor Surge-Basics, Mechanism*. Retrieved from <http://www.mechanicalengineeringsite.com/centrifugal-compressor-surge-basics-mechanism/>.
- Mecholic. (2016). *Advantages, Disadvantages And Applications of Centrifugal Compressor*. Retrieved from <https://www.mecholic.com/2016/07/advantages-disadvantages-applications-centrifugal-compressor.html#comment-form>.
- Mobil. (2019). *Once-through lubrication*. Retrieved from <https://club.mobilindustrial.com/glossary-of-lubrication-terms/w/glossary-of-terms/698/once-through-lubrication>
- Parker. (2018). *Parker O-Ring Handbook*. Retrieved from <https://www.parker.com/Literature/O-Ring%20Division%20Literature/ORD%205700.pdf>.
- Parr, A. (2011). *Air Compressors, Air Treatment and Pressure Regulation* (3rd ed.).
- Quincy Compressors. (2019). *How Do Oil-Free Air Compressors Work?*. Retrieved from <https://www.quincycompressor.com/how-do-oil-free-air-compressors-work/#Reciprocating>.

- Reading Plastic. (2019). *PTFE vs. Teflon: How Are These Plastics Related?*. Retrieved from <http://readingplastic.com/ptfe-vs-teflon/>.
- Samancioglu, M. (2016, March 9). *Comparison of Reciprocating and Centrifugal Compressors*. Retrieved from <https://www.linkedin.com/pulse/advantages-centrifugal-compressor-over-reciprocating-samancioglu/>.
- Schneider Electric, (2011). *Advantages and Disadvantages of Each Compressor Type*. Retrieved <http://energy.schneideruniversities.com/content/lessons/121//Compressed%20Air%20Systems%20II%20-%20Compressor%20Types/data/downloads/advantages%20and%20disadvantages%20-%20compressor%20types.pdf>.
- Scott, D. (2017, April 24). *How Does a Reciprocating Compressor Work?*. Retrieved from <https://sciencing.com/reciprocating-compressor-work-5002827.html>.
- Stewart, M. (2018). *Surface Production Operations: Volume Iv: Pumps and Compressors*. Gulf Professional Publishing. doi: <https://doi.org/10.1016/C2009-0-20243-1>
- Stosic, N., & Hanjalic, K. (1997, September). *Development and Optimization of Screw Machines With a Simulation Model - Part 1: Profile Generation*. Retrieved from <http://www.staff.city.ac.uk/~sj376/stosi197.htm>.
- The Compressed Air Blog. (2019, October 31). *How it Works: Centrifugal Compressors*. Retrieved from <https://www.thecompressedairblog.com/how-it-works-centrifugal-compressors>.
- The WC. (2019). *How oil-free rotary screw air compressors work*. Retrieved from <http://theworkshopcompressor.com/learn/compressor-types/rotary-screw-compressor/how-oil-free-rotary-screw-air-compressors-work/>.
- Ugural, A.C., & Fenster, S.K. (2012). *Advanced Mechanics of Materials and Applied Elasticity Fifth Edition*. Prentice Hall.
- VMAC. (2019, July 3). *Rotary Screw vs Reciprocating Air Compressors - Performance Differences*. Retrieved from <https://www.vmacair.com/blog/rotary-screw-vs-reciprocating-air-compressors-performance-differences/>.
- Wildenrad, F. (2019). *The Advantages Of Reciprocating Compressors*. Retrieved from <http://www.screenhaus.de/reciprocating-compressor/>.

## Appendix A: Glossary

C	Celsius
CARIES	Compressed Air Renewable Integrated Energy Storage
kW	Kilowatts
K	Kelvin
PSI	Pounds per square inch
PSIg	Pounds per square inch gauge
m	meter
mm	Millimeter
SCFM	Standard Cubic Feet per Minute
ACFM	Actual Cubic Feet per Minute
T	Temperature

## Appendix B: Cylinder Material Properties

### Carbon Steel, AISI 1095, as Rolled

<b>Price</b>		
By weight	.34 -.35	USD/LB
By volume	163-172	USD/ft <sup>3</sup>
<b>Mechanical Properties</b>		
Young's modulus	29-31	10 <sup>6</sup> psi
Yield strength	74-92.1	ksi
Tensile strength	125-155	ksi
Fatigue Strength at 10 <sup>7</sup> cycles	56-65.1	ksi
Fatigue Strength model (stress range)	56-65.1	ksi
Shear modulus	11.2-12.2	10 <sup>6</sup> psi
<b>Impact &amp; fracture Properties</b>		
Fracture toughness	41-69.2	ksi.in <sup>.5</sup>
<b>Thermal properties</b>		
Melting point	2350-2670	F
Maximum Service temperature	523-637	F
Minimum Service temperature	-45.4-0	F
Thermal Shock Resistance	381-504	F
Thermal expansion coefficient	6.11-7.5	ustrain/F

*Table 13, Carbon Steel, AISI 1095 Material Properties (CES edupack, 2019)*

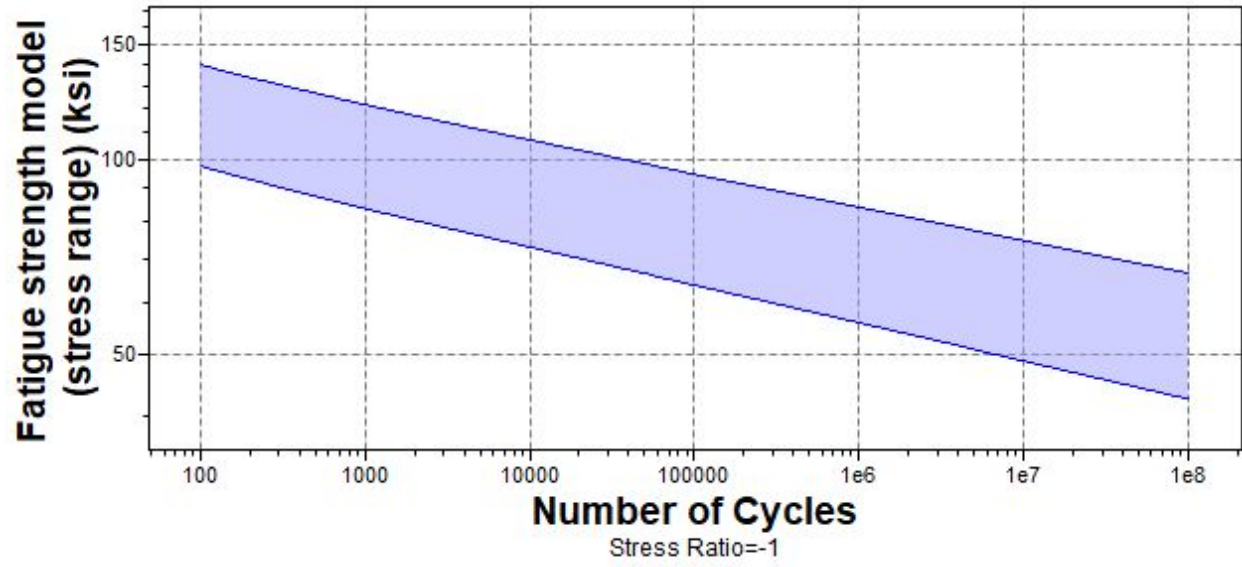


Figure 43, Carbon Steel, AISI 1095 Fatigue Strength Graph (CES edupack, 2019)

### Low Alloy Steel, AISI 5140, Oil Quenched & Tempered @ 650C

<b>Price</b>		
By weight	.34 -.35	USD/LB
By volume	168-177	USD/ft <sup>3</sup>
<b>Mechanical Properties</b>		
Young's modulus	30-31.5	10 <sup>6</sup> psi
Yield strength	87-105	ksi
Tensile strength	97.9-122	ksi
Fatigue Strength at 10 <sup>7</sup> cycles	47.1-55	ksi
Fatigue Strength model (stress range)	40.7-63.7	ksi
Shear modulus	11.6-12.3	10 <sup>6</sup> psi
<b>Impact &amp; fracture Properties</b>		
Fracture toughness	44.6-71.9	ksi.in <sup>.5</sup>
<b>Thermal properties</b>		
Melting point	2610-2740	F
Maximum Service temperature	1130-1180	F
Minimum Service temperature	-99 - -45	F
Thermal Shock Resistance	424-522	F
Thermal expansion coefficient	6.67-7.5	ustrain/F

*Table 14, Low Alloy Steel, AISI 5140 Material Properties (CES edupack, 2019)*

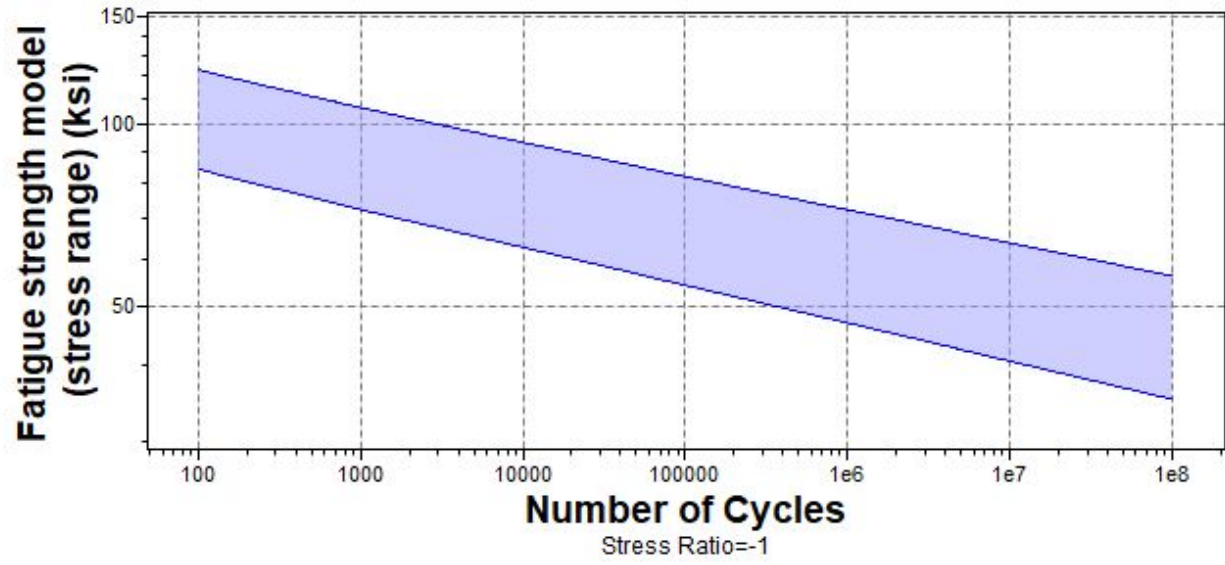


Figure 44, Low Alloy Steel, AISI 5140 Fatigue Strength Graph (CES edupack, 2019)

**Low Alloy Steel, AISI 4140, Normalized**

<b>Price</b>		
By weight	.38-.43	USD/LB
By volume	179-190	USD/ft <sup>3</sup>
<b>Mechanical Properties</b>		
Young's modulus	30-31.3	10 <sup>6</sup> psi
Yield strength	86.3-104	ksi
Tensile strength	93.3-163	ksi
Fatigue Strength at 10 <sup>7</sup> cycles	58.3-67.4	ksi
Fatigue Strength model (stress range)	50.8-77.5	ksi
Shear modulus	11.6-12.3	10 <sup>6</sup> psi
<b>Impact &amp; fracture Properties</b>		
Fracture toughness	61.9-97.4	ksi.in <sup>.5</sup>
<b>Thermal properties</b>		
Melting point	2610-2740	F
Maximum Service temperature	1140-1200	F
Minimum Service temperature	-90 - -36	F
Thermal Shock Resistance	426-534	F
Thermal expansion coefficient	6.39-7.5	ustrain/F

*Table 15, Low Alloy Steel, AISI 4140 Material Properties (CES edupack, 2019)*

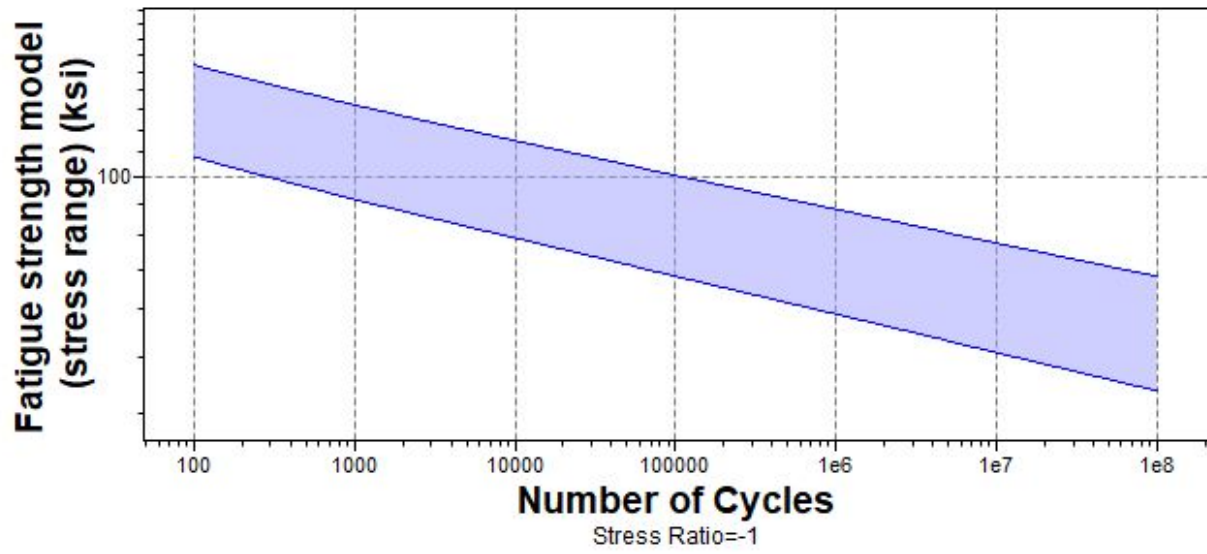


Figure 45, Low Alloy Steel, AISI 4140 Fatigue Strength Graph (CES edupack, 2019)

**Cast Iron, Pearlitic Malleable, EN GJMB 650-2**

<b>Price</b>		
By weight	.12-.19	USD/LB
By volume	52.7-88.1	USD/ft <sup>3</sup>
<b>Mechanical Properties</b>		
Young's modulus	22.2-27.1	10 <sup>6</sup> psi
Yield strength	462.4-85.7	ksi
Tensile strength	94.3-102	ksi
Fatigue Strength at 10 <sup>7</sup> cycles	40.6-46.4	ksi
Fatigue Strength model (stress range)	39.3-48	ksi
Shear modulus	8.7-10.9	10 <sup>6</sup> psi
<b>Impact &amp; fracture Properties</b>		
Fracture toughness	38.2-41.9	ksi.in <sup>.5</sup>
<b>Thermal properties</b>		
Melting point	2070-2470	F
Maximum Service temperature	662-842	F
Minimum Service temperature	-103-68	F
Thermal Shock Resistance	383-550	F
Thermal expansion coefficient	6.5-7.5	ustrain/F

*Table 16, Cast Iron, EN GJMB 650-2 Material Properties (CES edupack, 2019)*

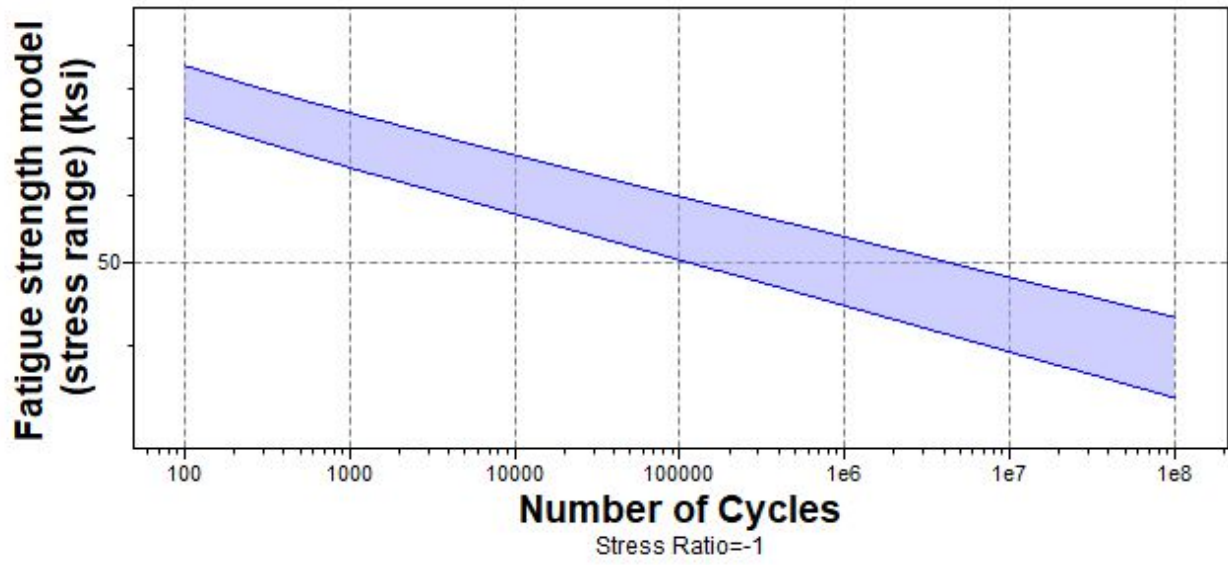


Figure 46, Cast Iron, Pearlitic Malleable Fatigue Strength Graph (CES edupack, 2019)

## Appendix C: Crankshaft Material Properties

### Low Alloy Steel, 300M (High Carbon), Quenched & Tempered

<b>Price</b>		
By weight	.49-.53	USD/LB
By volume	236-259	USD/ft <sup>3</sup>
<b>Mechanical Properties</b>		
Young's modulus	29-31	10 <sup>6</sup> psi
Yield strength	230-254	ksi
Tensile strength	280-310	ksi
Fatigue Strength at 10 <sup>7</sup> cycles	116-128	ksi
Fatigue Strength model (stress range)	109-136	ksi
Shear modulus	11-11.6	10 <sup>6</sup> psi
<b>Impact &amp; fracture Properties</b>		
Fracture toughness	45-52	ksi.in <sup>.5</sup>

Table 17, Low Alloy Steel, 300M Material Properties (CES edupack, 2019)

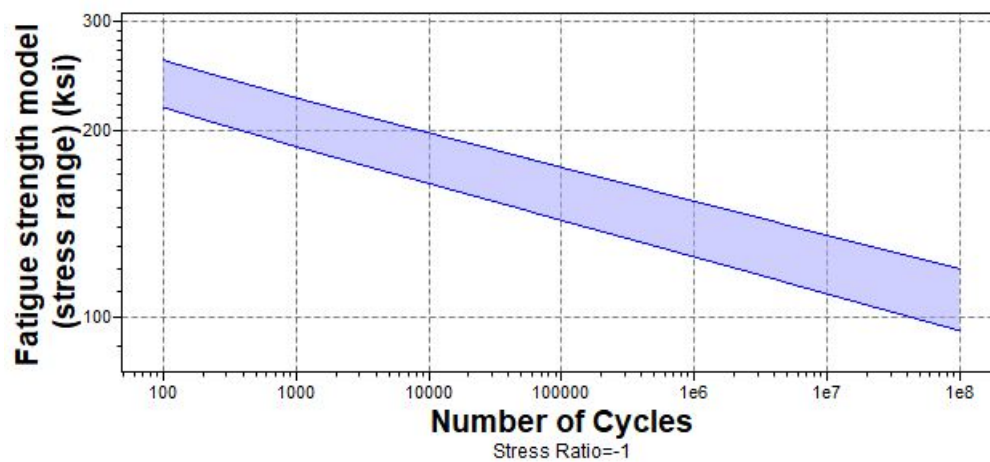


Figure 47, Low Alloy Steel, 300M Fatigue Strength Graph (CES edupack, 2019)

### Low alloy steel, AISI 9260, Oil quenched & tempered at 425C

<b>Price</b>		
By weight	.35-.37	USD/LB
By volume	170-181	USD/ft <sup>3</sup>
<b>Mechanical Properties</b>		
Young's modulus	29-31	10 <sup>6</sup> psi
Yield strength	196-240	ksi
Tensile strength	229-281	ksi
Fatigue Strength at 10 <sup>7</sup> cycles	85-99	ksi
Fatigue Strength model (stress range)	75-113	ksi
Shear modulus	11.3-12	10 <sup>6</sup> psi
<b>Impact &amp; fracture Properties</b>		
Fracture toughness	26-51	ksi.in <sup>.5</sup>

Table 18, Low Alloy Steel, AISI 9260 Material Properties (CES edupack, 2019)

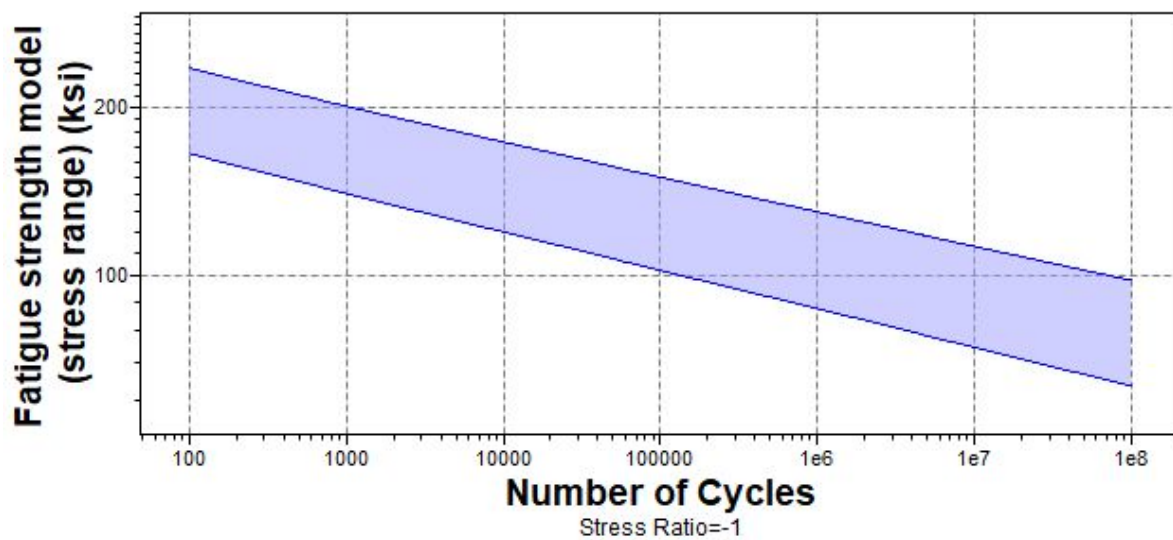


Figure 48, Low Alloy Steel, AISI 9260 Fatigue Strength Graph (CES edupack, 2019)

### Carbon steel, AISI 1095, oil quenched & tempered at 205C

<b>Price</b>		
By weight	.34-.35	USD/LB
By volume	163-172	USD/ft <sup>3</sup>
<b>Mechanical Properties</b>		
Young's modulus	29-31	10 <sup>6</sup> psi
Yield strength	107-133	ksi
Tensile strength	168-206	ksi
Fatigue Strength at 10 <sup>7</sup> cycles	69-80	ksi
Fatigue Strength model (stress range)	60-91	ksi
Shear modulus	11-12	10 <sup>6</sup> psi
<b>Impact &amp; fracture Properties</b>		
Fracture toughness	33-56	ksi.in <sup>.5</sup>

Table 19, Carbon Steel, AISI 1095 Material Properties (CES edupack, 2019)

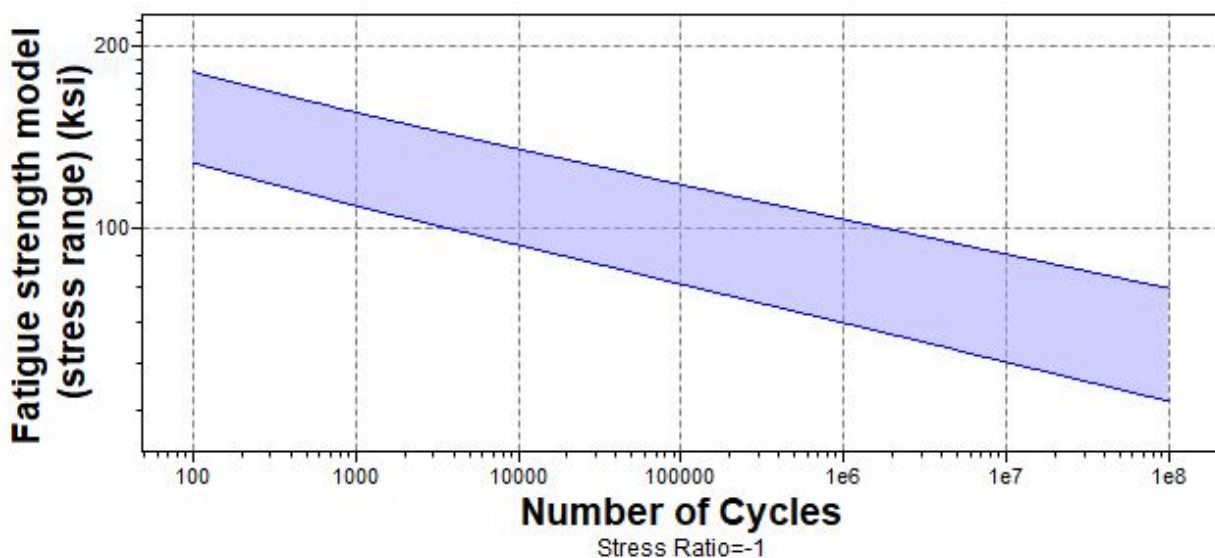
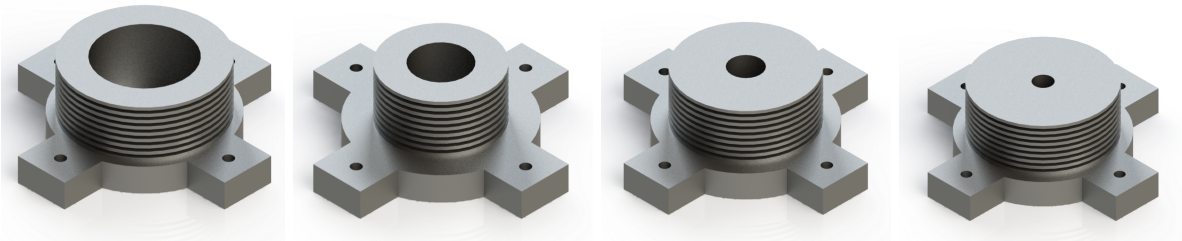


Figure 49, Carbon Steel, AISI 1095 Fatigue Strength Graph (CES edupack, 2019)

## Appendix D: CAD



*Figure 50, Piston Design Stages 1 (left) through 4 (right)*



*Figure 51, Cylinder Chamber Stages 1 (left) through 4 (right)*

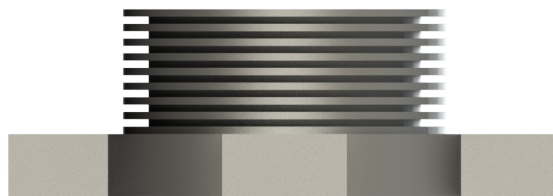


*Figure 52, Side View of Cylinder Chamber Highlighting Fins*

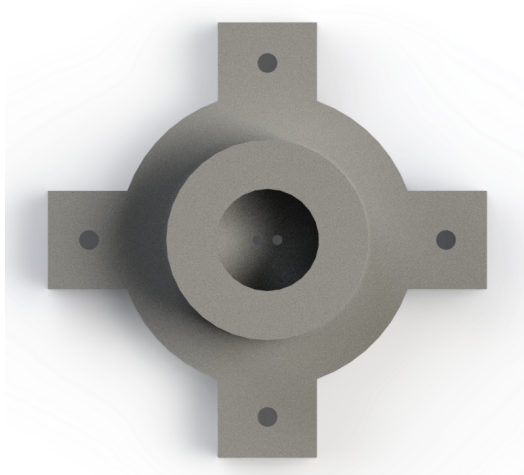


*Figure 53, Cylinder Chamber Top View Highlighting Valve Holes*

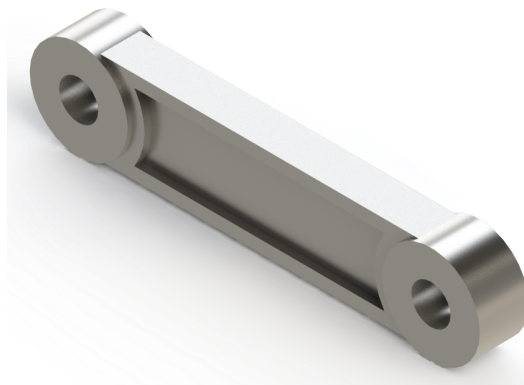


*Figure 54, Connecting Rod Design Stages 2-4*

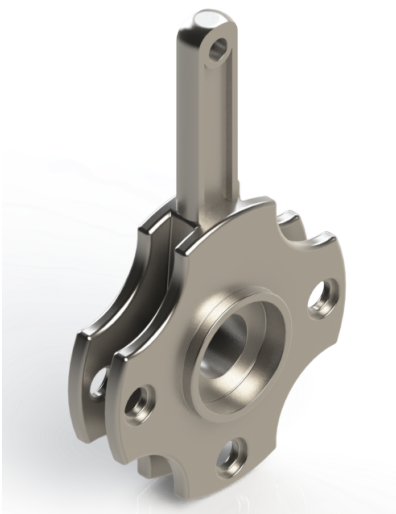


*Figure 55, Crankshaft Design*

## Appendix E: Failure Analysis of Cylinders

A structural analysis was performed on the cylinders in stages 1-4. Through the use of hand calculations, the maximum pressure present in each stage was applied to all surfaces on the inside of the cylinder head. This was done to ensure that the cylinders did not burst when this maximum pressure was reached. Additionally, the maximum stress experienced by each cylinder was also measured. Finally, the top outside surface of the cylinders was treated as fixed to more accurately model the component in the full assembly. The results for each stage are shown below in *Figures 56 to 63*.

### Total Deformation

#### Cylinder Stage 1 Pressure Total Deformation

The structural analysis for stage 1 involved applying the maximum pressure of **404kPa** to all surfaces on the inside of the cylinder. The result is shown below in *Figure 56*.

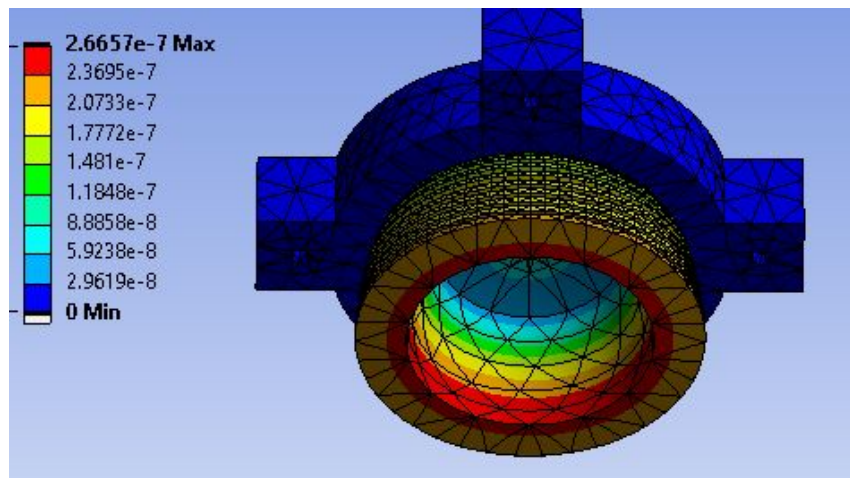


*Figure 56, Stage 1 Cylinder ANSYS Deformation*

When fully applied, the maximum deformation present was  **$2.6657 \times 10^{-7}$  m**. This amount of deformation is well within the allowable amount, and as a result, the cylinder was deemed structurally sound for stage 1.

#### Cylinder Stage 2 Pressure Total Deformation

The structural analysis for stage 2 involved applying the maximum pressure of **1616kPa** to all surfaces on the inside of the cylinder. The result is shown below in *Figure 57*.

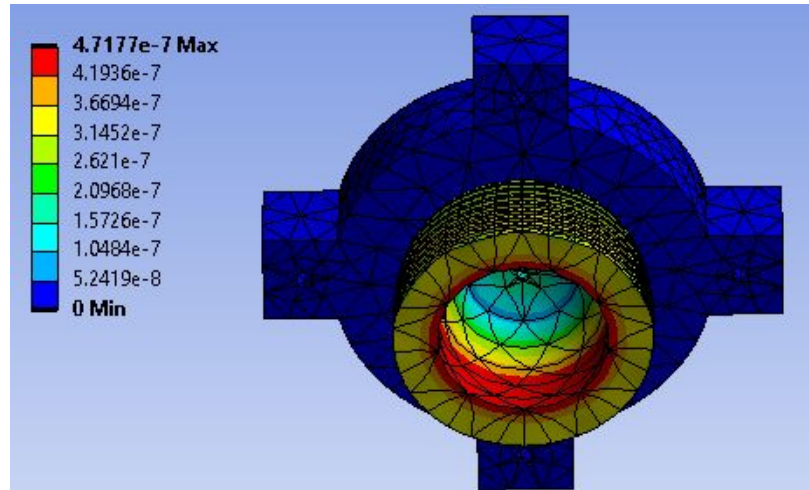


Figure 57, Stage 2 Cylinder ANSYS Deformation

When fully applied, the maximum deformation present was  $4.7177 \times 10^{-7}$  m. This amount of deformation is well within the allowable amount, and as a result, the cylinder was deemed structurally sound for stage 2.

#### Cylinder Stage 3 Pressure Total Deformation

The structural analysis for stage 3 involved applying the maximum pressure of **6464kPa** to all surfaces on the inside of the cylinder. The result is shown below in Figure 58.

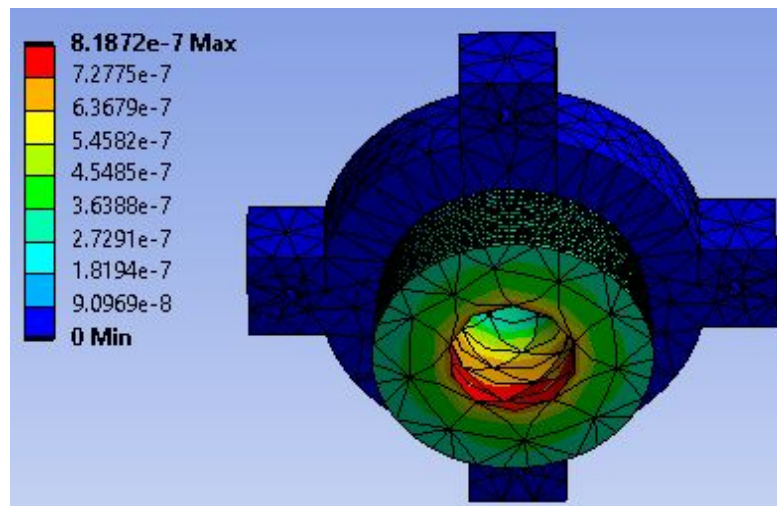
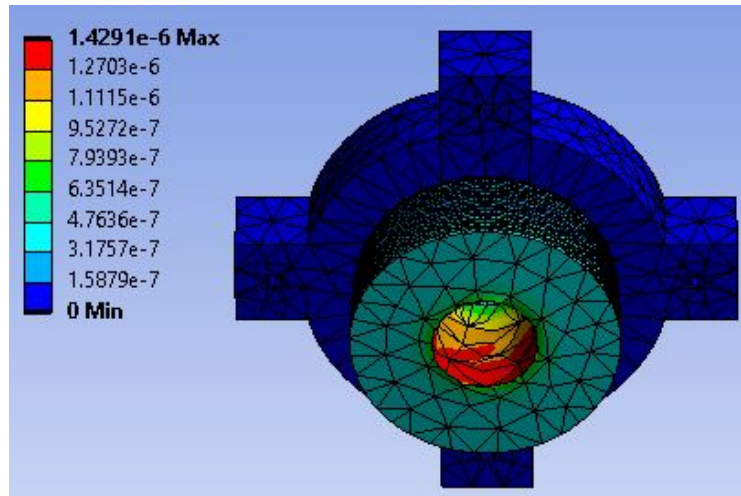


Figure 58, Stage 3 Cylinder ANSYS Deformation

When fully applied, the maximum deformation present was  $8.1872 \times 10^{-7}$  m. This amount of deformation is well within the allowable amount, and as a result, the cylinder was deemed structurally sound for stage 3.

### Cylinder Stage 4 Pressure Total Deformation

The structural analysis for stage 4 involved applying the maximum pressure of **20788kPa** to all surfaces on the inside of the cylinder. The result is shown below in *Figure 59*.



*Figure 59, Stage 4 Cylinder ANSYS Deformation*

When fully applied, the maximum deformation present was **1.4291 x 10<sup>-6</sup> m**. This amount of deformation is well within the allowable amount, and as a result, the cylinder was deemed structurally sound for stage 4.

### **Total Stress (Von-Mises)**

#### Cylinder Stage 1 Pressure Total Stress (Von-Mises)

The structural analysis for stage 1 involved applying the maximum pressure of **404kPa** to all surfaces on the inside of the cylinder. The result is shown below in *Figure 60*.

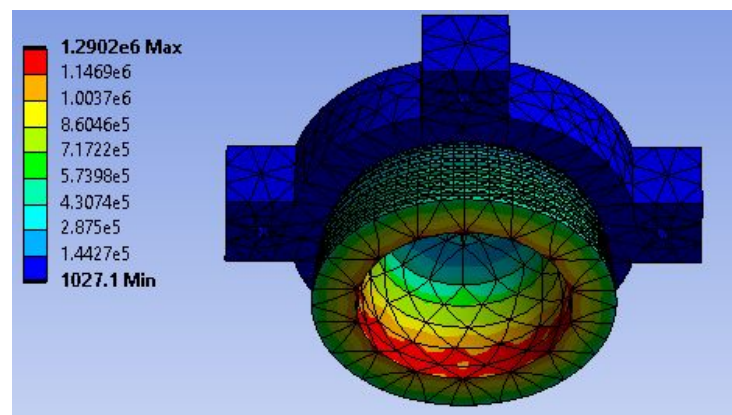


*Figure 60, Stage 1 Cylinder ANSYS Stress*

When fully applied, the equivalent Von-Mises Stress present was  **$1.2902 \times 10^6$  Pa**. The maximum equivalent stress experienced by the cylinder is far below that of 5140 steel's yield stress, 600MPa, and thus it can be determined that the component can support this load safely.

#### Cylinder Stage 2 Pressure Total Stress (Von-Mises)

The structural analysis for stage 2 involved applying the maximum pressure of **1616kPa** to all surfaces on the inside of the cylinder. The result is shown below in *Figure 61*.

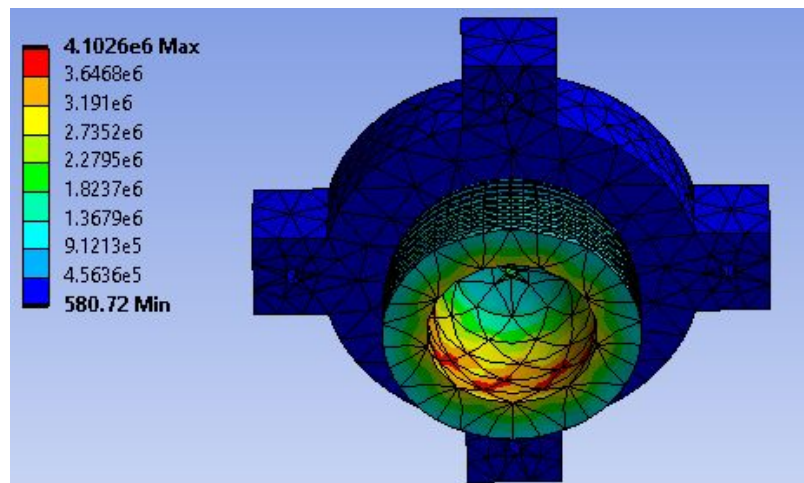


*Figure 61, Stage 2 Cylinder ANSYS Stress*

When fully applied, the equivalent Von-Mises Stress present was  **$4.1026 \times 10^6$  Pa**. The maximum equivalent stress experienced by the cylinder is far below that of both 5140 steel's yield stress, 600MPa, and thus it can be determined that the component can support this load safely.

#### Cylinder Stage 3 Pressure Total Stress (Von-Mises)

The structural analysis for stage 3 involved applying the maximum pressure of **6464kPa** to all surfaces on the inside of the cylinder. The result is shown below in *Figure 62*.

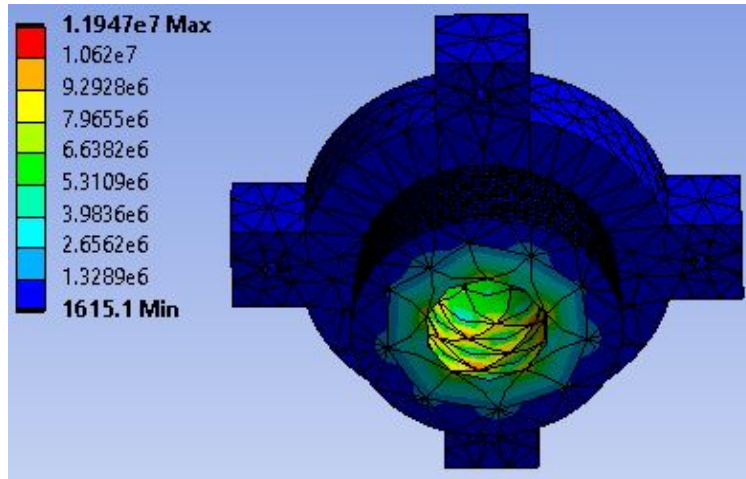


*Figure 62, Stage 3 Cylinder ANSYS Stress*

When fully applied, the equivalent Von-Mises Stress present was  **$1.1947 \times 10^7$  Pa**. The maximum equivalent stress experienced by the cylinder is far below that of 5140 steel's yield stress, 600MPa, and thus it can be determined that the component can support this load safely.

#### Cylinder Stage 4 Pressure Total Stress (Von-Mises)

The structural analysis for stage 4 involved applying the maximum pressure of **20788kPa** to all surfaces on the inside of the cylinder. The result is shown below in *Figure 63*.

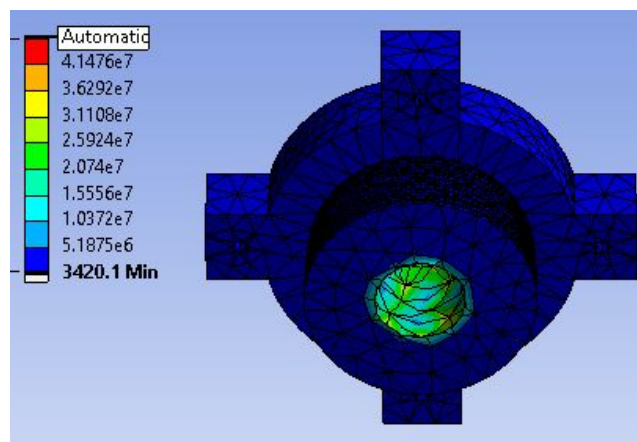


*Figure 63, Stage 4 Cylinder ANSYS Stress*

When fully applied, the equivalent Von-Mises Stress present was about  **$4.1476 \times 10^7$  Pa**. The maximum equivalent stress experienced by the cylinder is far below that of 5140 steel's yield stress, 600MPa, and thus it can be determined that the component can support this load safely.

## Appendix F: Failure Analysis of Piston

Additional ANSYS structural simulations were conducted on the aluminum piston heads for all four stages of the compressor. This was primarily done to ensure that the thin stem attaching the piston head to the connecting rod would not buckle when experiencing the maximum pressure in each stage. Additionally, the piston was fixed at the point where the dowel pin would be inserted for practicality purposes. The results of these simulations are found in *Figure 64-71* below.

### Total Deformation

#### Piston Stage 1 Pressure

The structural analysis for stage 1 involved applying the maximum pressure of **404kPa** to the entire top surface of the piston head. The result is shown below in *Figure 64*.

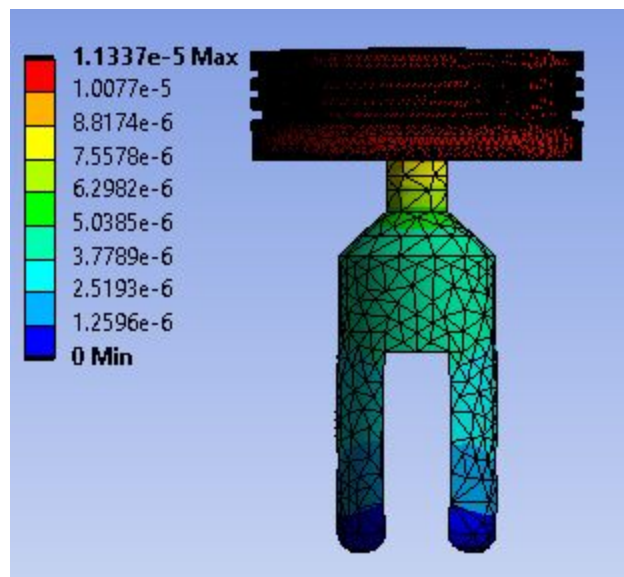


*Figure 64, Piston Stage 1 Deformation*

When fully applied, the maximum deformation present was  **$1.1337 \times 10^{-5} \text{m}$** . This amount of deformation is well within the allowable amount, and as a result, the piston was deemed structurally sound for stage 1.

#### Piston Stage 2 Pressure

The structural analysis for stage 2 involved applying the maximum pressure of **1616kPa** to the entire top surface of the piston head. The result is shown below in *Figure 65*.

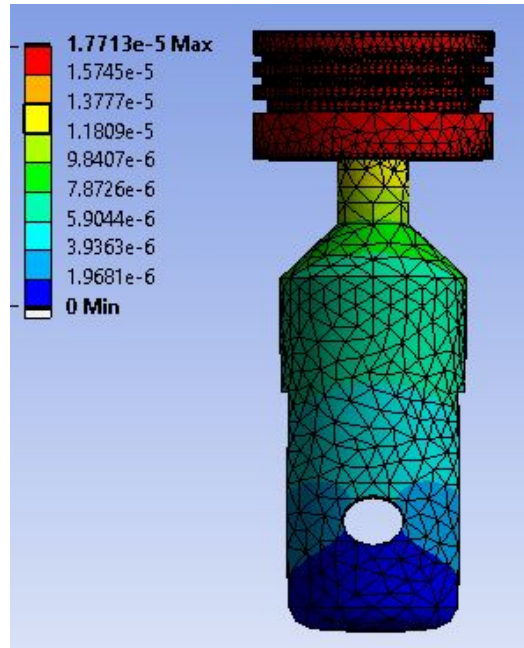


*Figure 65, Piston Stage 2 Deformation*

When fully applied, the maximum deformation present was  $1.7713 \times 10^{-5}$  m. This amount of deformation is well within the allowable amount, and as a result, the piston was deemed structurally sound for stage 2.

### Piston Stage 3 Pressure

The structural analysis for stage 3 involved applying the maximum pressure of **6464kPa** to the entire top surface of the piston head. The result is shown below in *Figure 66*.

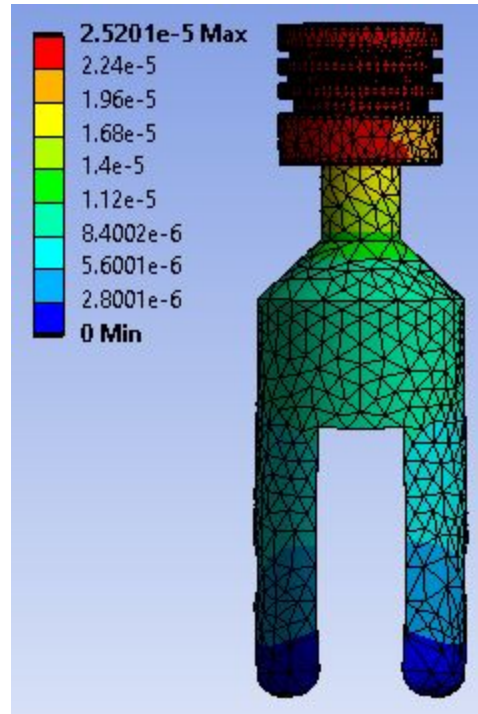


*Figure 66, Piston Stage 3 Deformation*

When fully applied, the maximum deformation present was  $2.5201 \times 10^{-5} \text{ m}$ . This amount of deformation is well within the allowable amount, and as a result, the piston was deemed structurally sound for stage 3.

#### Piston Stage 4 Pressure

The structural analysis for stage 4 involved applying the maximum pressure of **207,88kPa** to the entire top surface of the piston head. The result is shown below in *Figure 67*.

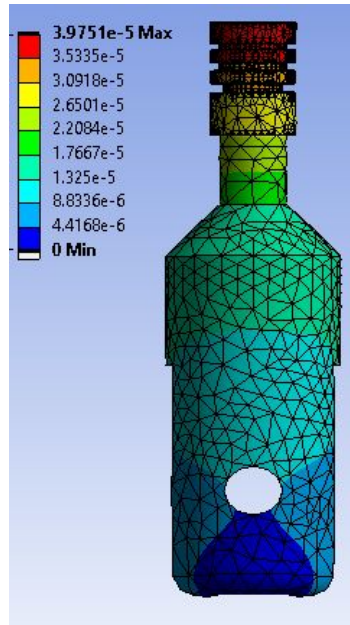


Figure 67, Piston Stage 4 Deformation

When fully applied, the maximum deformation present was  $3.9751 \times 10^{-5}$  m. This amount of deformation is well within the allowable amount, and as a result, the piston was deemed structurally sound for stage 4.

## Total Stress (Von-Mises)

### Piston Stage 1 Pressure Total Stress (Von-Mises)

The structural analysis for stage 1 involved applying the maximum pressure of **404kPa** to the entire top surface of the piston head. The result is shown below in *Figure 68*.

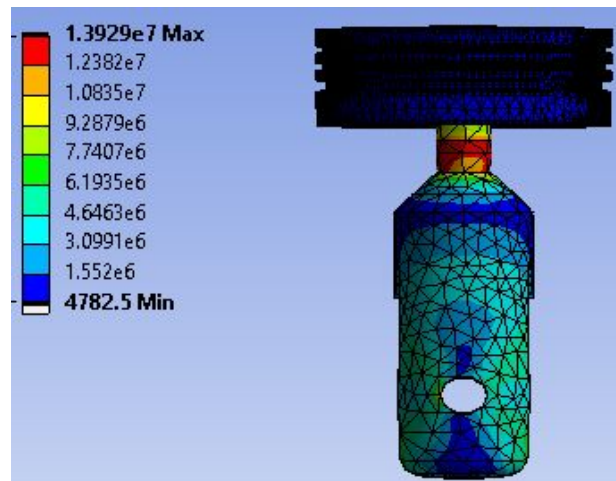
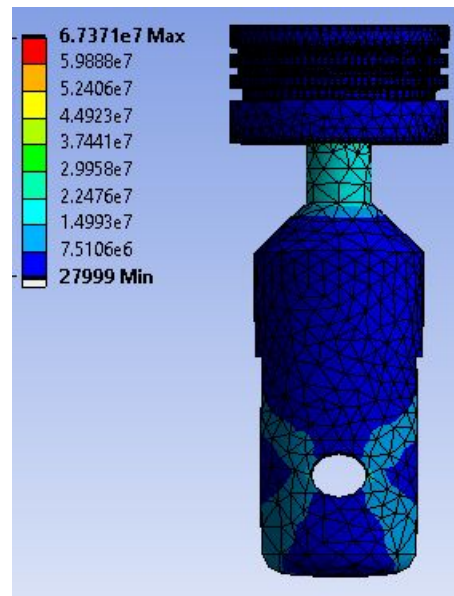


Figure 68, Piston Stage 1 Stress

When fully applied, the equivalent Von-Mises Stress present was about **1.3929 x 10<sup>7</sup> Pa**. The maximum equivalent stress experienced by the piston is below 6061 aluminum's yield stress, 276MPa, and thus it can be determined that the component can support this load safely.

#### Piston Stage 2 Pressure Total Stress (Von-Mises)

The structural analysis for stage 2 involved applying the maximum pressure of **1616kPa** to the entire top surface of the piston head. The result is shown below in *Figure 69*.



*Figure 69, Piston Stage 2 Stress*

When fully applied, the equivalent Von-Mises Stress present was about **6.7371 x 10<sup>7</sup> Pa**. The maximum equivalent stress experienced by the piston is below 6061 aluminum's yield stress, 276MPa, and thus it can be determined that the component can support this load safely.

#### Piston Stage 3 Pressure Total Stress (Von-Mises)

The structural analysis for stage 3 involved applying the maximum pressure of **6464kPa** to the entire top surface of the piston head. The result is shown below in *Figure 70*.

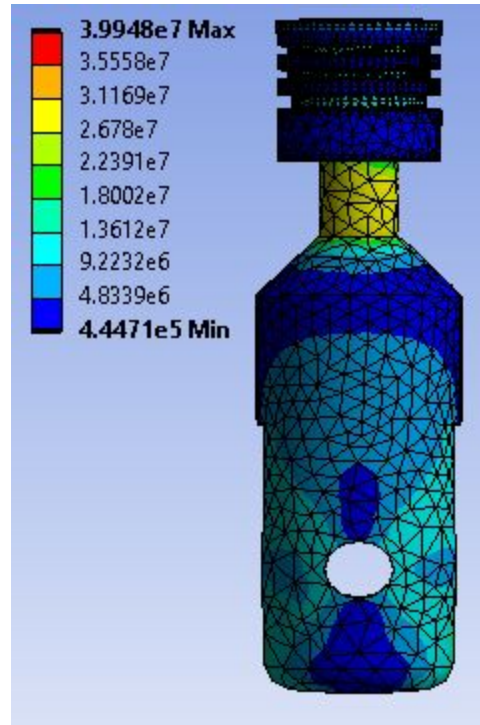


*Figure 70, Piston Stage 3 Stress*

When fully applied, the equivalent Von-Mises Stress present was about **3.9948 x 10<sup>7</sup> Pa**. The maximum equivalent stress experienced by the piston is below 6061 aluminum's yield stress, 276MPa, and thus it can be determined that the component can support this load safely.

#### Piston Stage 4 Pressure Total Stress (Von-Mises)

The structural analysis for stage 4 involved applying the maximum pressure of **20788kPa** to the entire top surface of the piston head. The result is shown below in *Figure 71*.

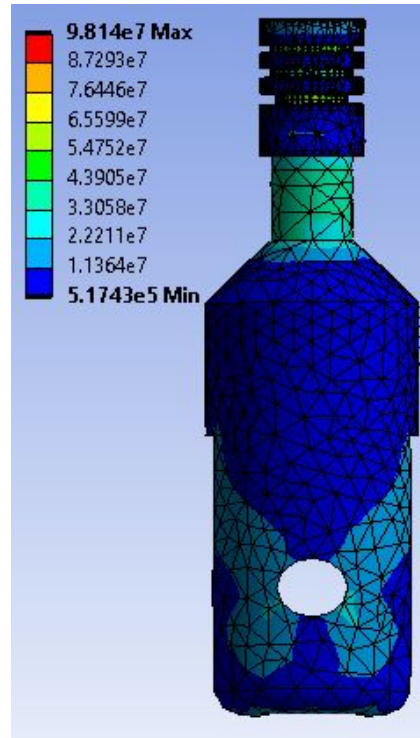


*Figure 71, Piston Stage 4 Stress*

When fully applied, the equivalent Von-Mises Stress present was about  $9.8140 \times 10^7$  Pa. The maximum equivalent stress experienced by the piston is below 6061 aluminum's yield stress, 276MPa, and thus it can be determined that the component can support this load safely.

## Appendix G: Failure Analysis of Connecting Rods

ANSYS structural analyses were also conducted on the connecting rods for all four stages of the compressor. The design of all four rods are relatively similar, but the varying pressures in each stage warranted a full analysis of all of them.

The first set of simulations conducted dealt with the load applied on the connecting rod from the piston at the maximum angle of deflection between the piston head and connecting rod. This angle was measured to be about 3 degrees, and as a result, the total pressure in each stage was decomposed into x and y components to more accurately model this load. For practicality purposes, the bottom of the connecting rod which attaches to the master rod assembly was treated as a fixed point.

The second set of simulations was mainly done to model the most intense scenario. The maximum pressure in each stage was distributed along the one side of each connecting rod, to act on the component at a 90-degree angle. Additionally, the rod was fixed on one side. The results for all of these simulations are found below in *Figures 72-87*.

### Total Deformation - Load Applied from Piston Head

#### Connecting Rod Stage 1 Load from Piston

The structural analysis for stage 1 involved applying the maximum pressure of **404kPa** to the top surface of the connecting rod. Using an angle of deflection of 3 degrees between the piston head and the connecting rod, x and y component forces were able to be determined for the **404kPa** pressure. These values were **403kPa** in the y-direction and **21 kPa** in the x-direction. The result is shown below in *Figure 72*

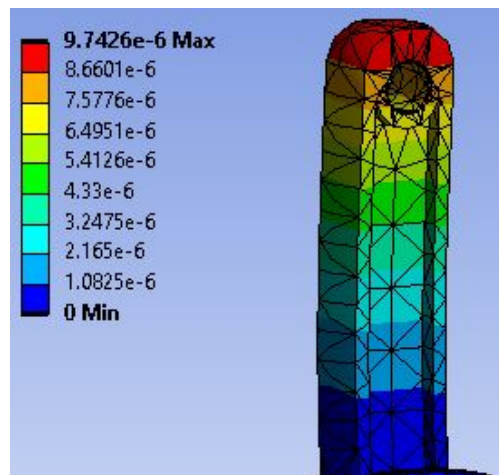


*Figure 72, Master Rod to Piston Deformation Stage 1*

When fully applied, the maximum deformation present was  $9.7426 \times 10^{-6} \text{ m}$ . This amount of deformation is well within the allowable amount, and as a result, the connecting rod was deemed structurally sound for stage 1.

#### Connecting Rod Stage 2 Load from Piston

The structural analysis for stage 2 involved applying the maximum pressure of **1,616kPa** to the top surface of the connecting rod. Using an angle of deflection of 3 degrees between the piston head and the connecting rod, x and y component forces were able to be determined for the **1,616kPa** pressure. These values were **1,614kPa** in the x-direction and **85kPa** in the y-direction. The result is shown below in *Figure 73*.

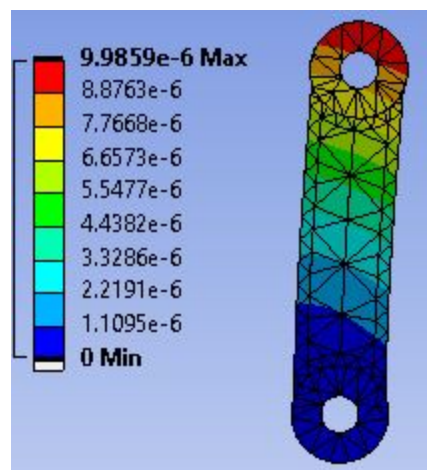


*Figure 73, Connecting Rod to Piston Deformation Stage 2*

When fully applied, the maximum deformation present was  $9.9859 \times 10^{-6} \text{ m}$ . This amount of deformation is well within the allowable amount, and as a result, the connecting rod was deemed structurally sound for stage 2.

#### Connecting Rod Stage 3 Load from Piston

The structural analysis for stage 3 involved applying the maximum pressure of **6464kPa** to the top surface of the connecting rod. Using an angle of deflection of 3 degrees between the piston head and the connecting rod, x and y component forces were able to be determined for the **6464kPa** pressure. These values were **6455kPa** in the y-direction and **338kPa** in the x-direction. The result is shown below in *74*.

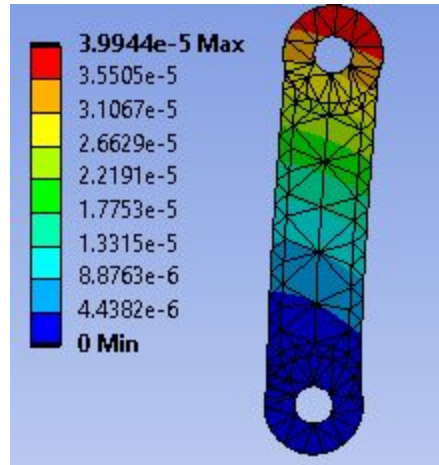


Figure 74, Connecting Rod to Piston Deformation Stage 3

When fully applied, the maximum deformation present was  $3.9944 \times 10^{-5}$  m. This amount of deformation is well within the allowable amount, and as a result, the connecting rod was deemed structurally sound for stage 3.

#### Connecting Rod Stage 4 Load from Piston

The structural analysis for stage 3 involved applying the maximum pressure of **20788kPa** to the top surface of the connecting rod. Using an angle of deflection of 3 degrees between the piston head and the connecting rod, x and y component forces were able to be determined for the **20788kPa** pressure. These values were **20760kPa** in the y-direction and **1088kPa** in the x-direction. The result is shown below in *Figure 75*.

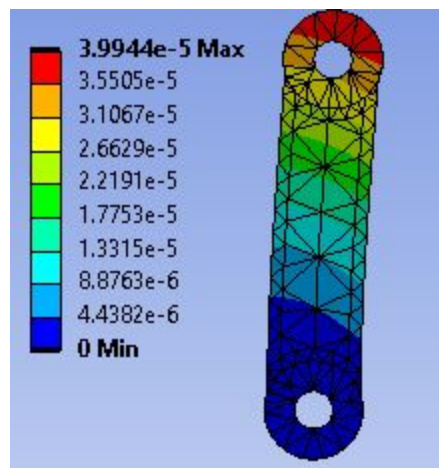


Figure 75, Connecting Rod to Piston Deformation Stage 4

When fully applied, the maximum deformation present was  $9.8135 \times 10^{-5}$  m. This amount of deformation is well within the allowable amount, and as a result, the connecting rod was deemed structurally sound for stage four.

## Total Stress (Von-Mises)

### Connecting Rod Stage 1 Load from Piston

The structural analysis for stage 1 involved applying the maximum pressure of **404kPa** to one side of the connecting rod. The same 3 degree angle was used to calculate the x and y components of the stress. Simulation provided a result of **403kPa** in the y-direction and **21kPa** in the x-direction. The result is shown below in *Figure 76*.

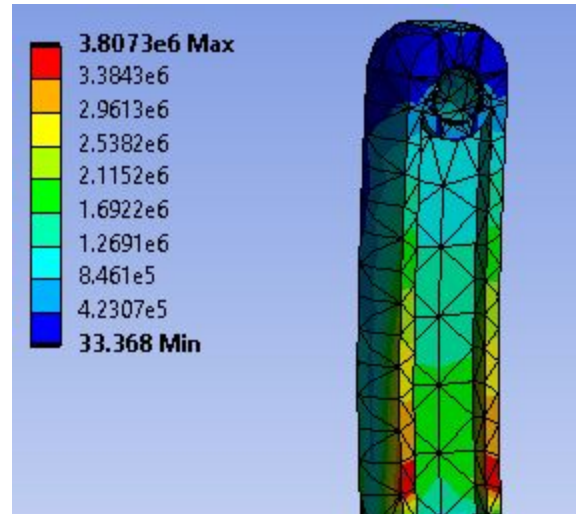


*Figure 76, Master Rod to Piston Stress Stage 1*

When fully applied, the equivalent Von-Mises Stress present was about **3.8073 x 10<sup>6</sup> Pa**. The maximum equivalent stress experienced by the connecting rod is far below that of Low Alloy Steel 300M's yield stress, 738MPa, and thus it can be determined that the component can support this load safely.

### Connecting Rod Stage 2 Load from Piston

The structural analysis for stage 2 involved applying the maximum pressure of **1616kPa** to one side of the connecting rod. The same 3 degree angle was used to calculate the x and y components of the stress. Simulation provided a result of **1614kPa** in the y-direction and **85kPa** in the x-direction. The result is shown below in *Figure 77*.

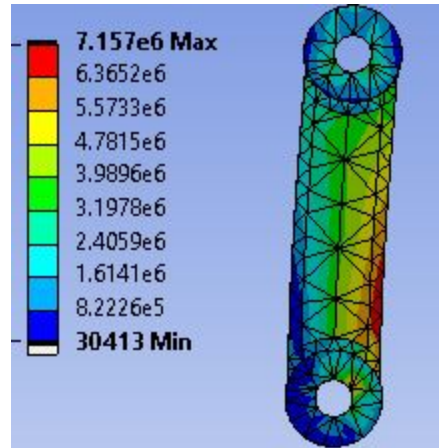


Figure 77, Connecting Rod to Piston Stress Stage 2

When fully applied, the equivalent Von-Mises Stress present was about **7.1570 x 10<sup>6</sup> Pa**. The maximum equivalent stress experienced by the connecting rod is far below that of Low Alloy Steel 300M's yield stress, 738MPa, and thus it can be determined that the component can support this load safely.

#### Connecting Rod Stage 3 Load from Piston

The structural analysis for stage 3 involved applying the maximum pressure of **6464kPa** to one side of the connecting rod. The same 3 degree angle was used to calculate the x and y components of the stress. Simulation provided a result of **6455kPa** in the y-direction and **338kPa** in the x-direction. The result is shown below in *Figure 78*.

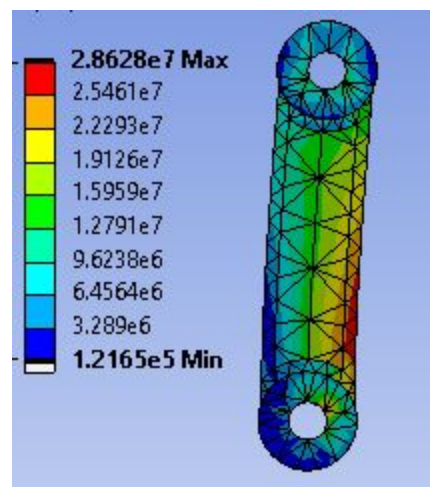


Figure 78, Connecting Rod to Piston Stress Stage 3

When fully applied, the equivalent Von-Mises Stress present was about **2.8628 x 10<sup>7</sup> Pa**. The maximum equivalent stress experienced by the connecting rod is far below that

of Low Alloy Steel 300M's yield stress, 738MPa, and thus it can be determined that the component can support this load safely.

#### Connecting Rod Stage 4 Load from Piston

The structural analysis for stage 4 involved applying the maximum pressure of **20788kPa** to one side of the connecting rod. The same 3 degree angle was used to calculate the x and y components of the stress. Simulation provided a result of **20760kPa** in the y-direction and **1088kPa** in the x-direction. The result is shown below in *Figure 79*.

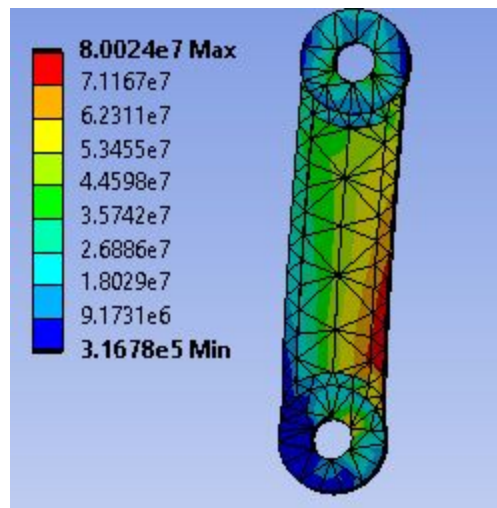


*Figure 79, Connecting Rod to Piston Stress Stage 4*

When fully applied, the equivalent Von-Mises Stress present was about **8.0024 x 10<sup>7</sup> Pa**. The maximum equivalent stress experienced by the connecting rod is far below that of Low Alloy Steel 300M's yield stress, 738MPa, and thus it can be determined that the component can support this load safely.

### **Total Deformation - Perpendicular Load**

#### Connecting Rod Stage 1

The structural analysis for stage 1 involved applying the maximum pressure of **404 kPa** to one side of the connecting rod while keeping one end fixed. The result is shown below in *Figure 80*.

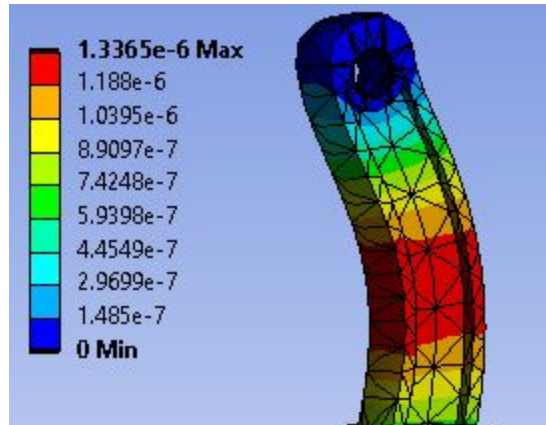


Figure 80, Master Rod Deformation Stage 1

When fully applied, the maximum deformation present was  $1.3365 \times 10^{-6} \text{ m}$ . This amount of deformation is well within the allowable amount, and as a result, the connecting was deemed structurally stable for stage 1.

### Connecting Rod Stage 2

The structural analysis for stage 2 involved applying the maximum pressure of **1616 kPa** to one side of the connecting rod while keeping one end fixed. The result is shown below in *Figure 81*.

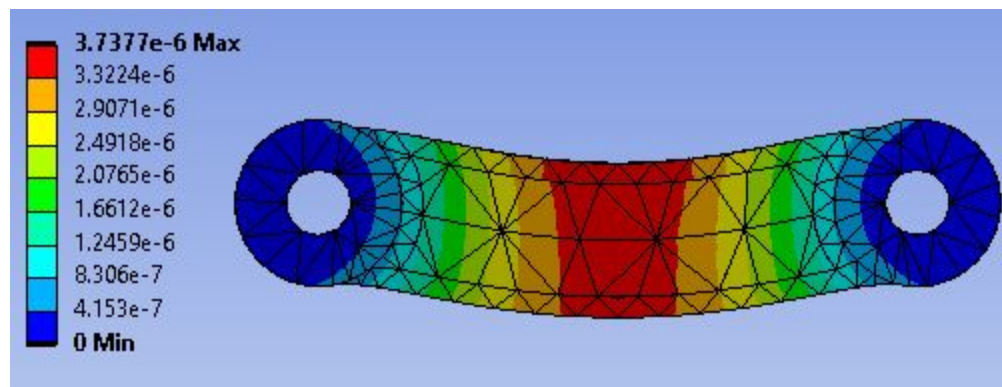
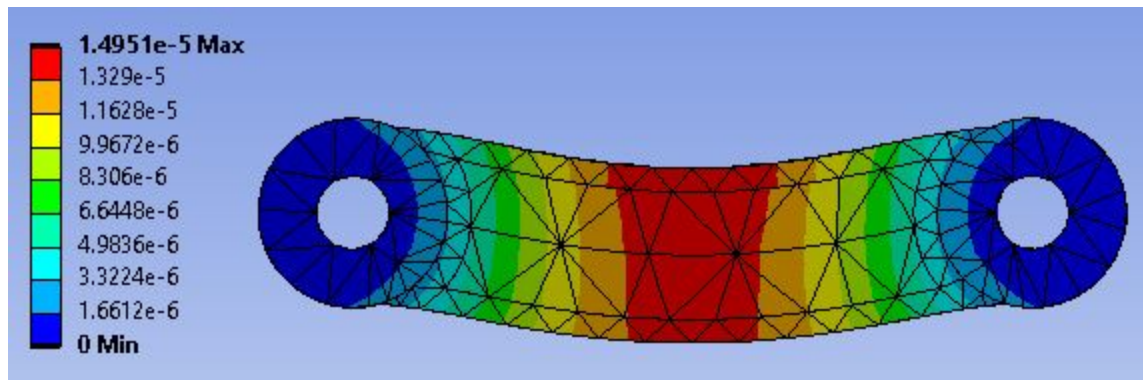


Figure 81, Connecting Rod Deformation Stage 2

When fully applied, the maximum deformation present was  $3.7377 \times 10^{-6} \text{ m}$ . This amount of deformation is well within the allowable amount, and as a result, the connecting was deemed structurally stable for stage 2.

### Connecting Rod Stage 3

The structural analysis for stage 3 involved applying the maximum pressure of **6464 kPa** to one side of the connecting rod, while keeping one end fixed. The result is shown below in *Figure 82*.



*Figure 82, Connecting Rod Deformation Stage 3*

When fully applied, the maximum deformation present was  **$1.4951 \times 10^{-5}$  m**. This amount of deformation is well within the allowable amount, and as a result, the connecting was deemed structurally stable for stage 3.

#### Connecting Rod Stage 4

The structural analysis for stage 4 involved applying the maximum pressure of **20788 kPa** to one side of the connecting rod, while keeping one end fixed. The result is shown below in *Figure 83*.

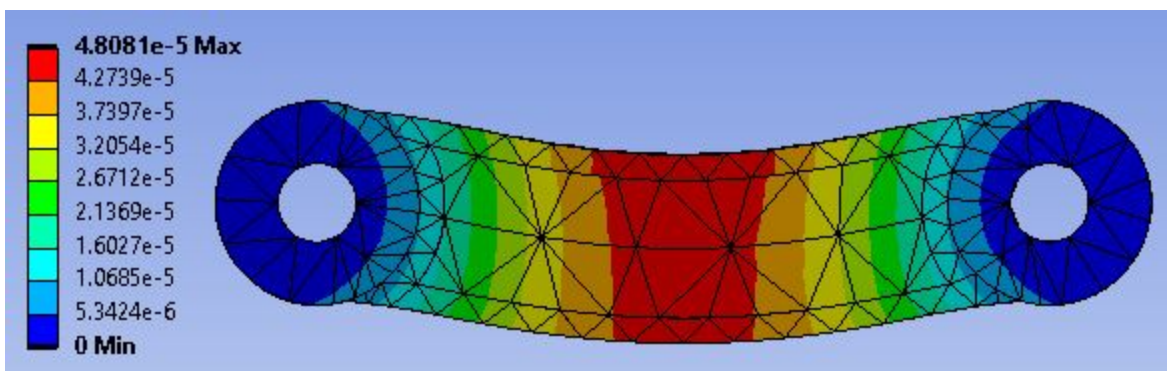


*Figure 83, Connecting Rod Deformation Stage 4*

When fully applied, the maximum deformation present was  **$4.8081 \times 10^{-5}$  m**. This amount of deformation is well within the allowable amount, and as a result, the connecting was deemed structurally stable for stage 4.

### **Total Stress (Von-Mises)**

### Connecting Rod Stage 1

The structural analysis for stage 1 involved applying the maximum pressure of **404 kPa** to one side of the connecting rod while keeping one end fixed. The result is shown below in *Figure 84*.

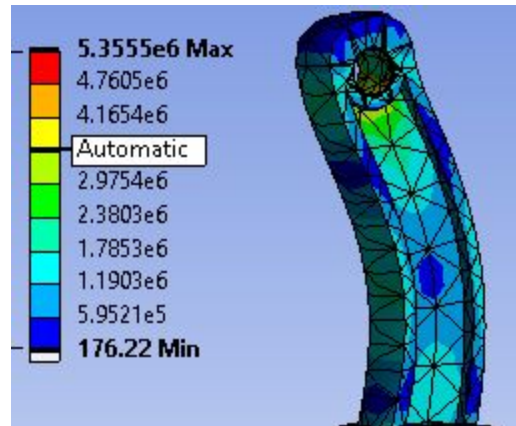


*Figure 84, Master Rod Stress*

When fully applied, the equivalent Von-Mises Stress present was about **5.3555 x 10<sup>6</sup> Pa**. The maximum equivalent stress experienced by the connecting rod is far below that of Low Alloy Steel 300M's yield stress, 738MPa, and thus it can be determined that the component can support this load safely.

### Connecting Rod Stage 2

The structural analysis for stage 2 involved applying the maximum pressure of **1616 kPa** to one side of the connecting rod while keeping one end fixed. The result is shown below in *Figure 85*.

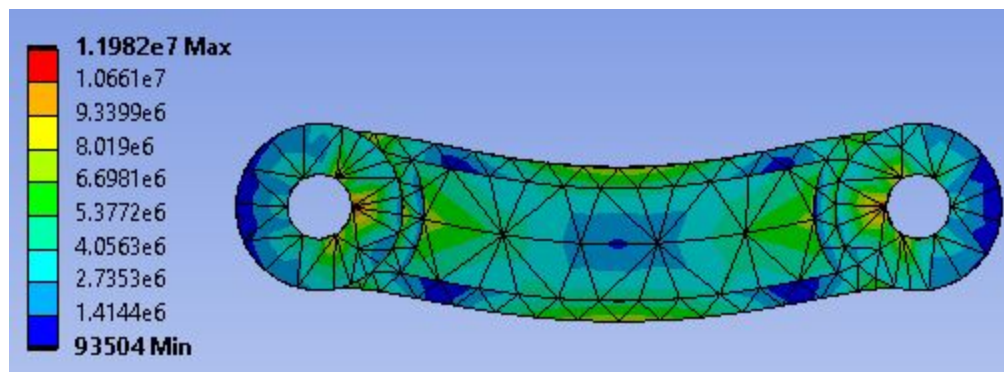


*Figure 85, Connecting Rod Stress Stage 2*

When fully applied, the equivalent Von-Mises Stress present was about **1.1982 x 10<sup>7</sup> Pa**. The maximum equivalent stress experienced by the connecting rod is far below that

of Low Alloy Steel 300M's yield stress, 738MPa, and thus it can be determined that the component can support this load safely.

### Connecting Rod Stage 3

The structural analysis for stage 3 involved applying the maximum pressure of **6464 kPa** to one side of the connecting rod while keeping one end fixed. The result is shown below in *Figure 86*.

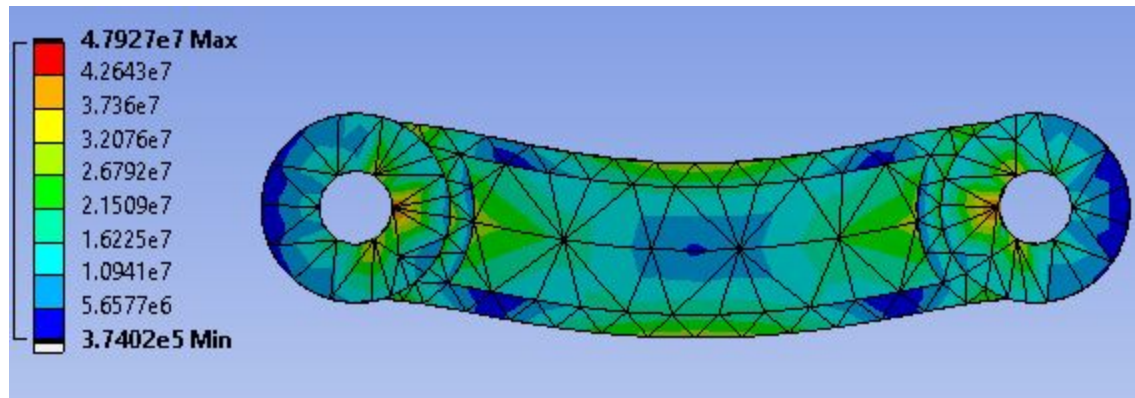


*Figure 86, Connecting Rod Stress Stage 3*

When fully applied, the equivalent Von-Mises Stress present was about **4.7927 x 10<sup>7</sup> Pa**. The maximum equivalent stress experienced by the connecting rod is far below that of Low Alloy Steel 300M's yield stress, 738MPa, and thus it can be determined that the component can support this load safely.

### Connecting Rod Stage 4

The structural analysis for stage 4 involved applying the maximum pressure of **20788 kPa** to one side of the connecting rod while keeping one end fixed. The result is shown below in *Figure 87*,

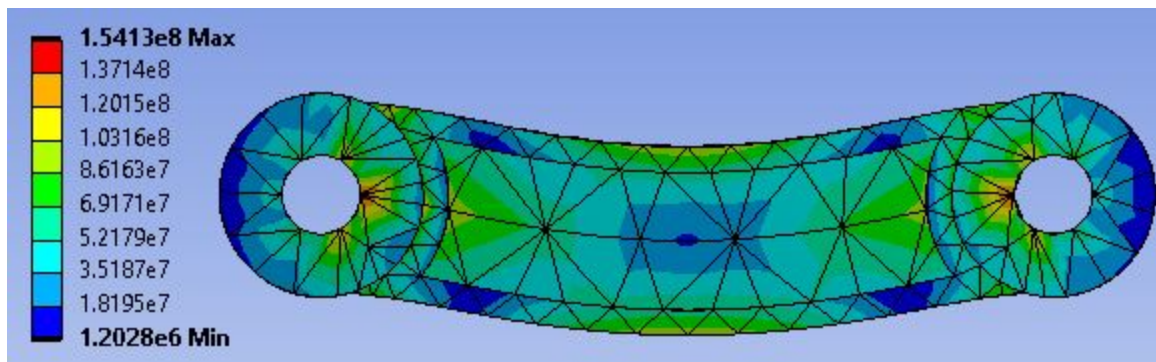


*Figure 87, Connecting Rod Stress Stage 4*

When fully applied, the equivalent Von-Mises Stress present was about **1.5413 x 10<sup>8</sup> Pa**. The maximum equivalent stress experienced by the connecting rod is far below that of Low Alloy Steel 300M's yield stress, 738MPa, and thus it can be determined that the component can support this load safely.